

Prox1 Regulates the Subtype-Specific Development of Caudal Ganglionic Eminence-Derived GABAergic Cortical Interneurons

Goichi Miyoshi,¹ Allison Young,¹ Timothy Petros,¹ Theofanis Karayannis,¹ Melissa McKenzie Chang,¹ Alfonso Lavado,² Tomohiko Iwano,³ Miho Nakajima,⁴ Hiroki Taniguchi,⁵ Z. Josh Huang,⁵ Nathaniel Heintz,⁴ Guillermo Oliver,² Fumio Matsuzaki,³ Robert P. Machold,¹ and Gord Fishell¹

¹Department of Neuroscience and Physiology, NYU Neuroscience Institute, Smilow Research Center, New York University School of Medicine, New York, New York 10016, ²Department of Genetics & Tumor Cell Biology, St. Jude Children's Research Hospital, Memphis, Tennessee 38105, ³Laboratory for Cell Asymmetry, RIKEN Center for Developmental Biology, Kobe 650-0047, Japan, ⁴Laboratory of Molecular Biology, Howard Hughes Medical Institute, GENSAT Project, The Rockefeller University, New York, New York 10065, and ⁵Cold Spring Harbor Laboratory, Cold Spring Harbor, New York 11724

Neurogliaform (RELN+) and bipolar (VIP+) GABAergic interneurons of the mammalian cerebral cortex provide critical inhibition locally within the superficial layers. While these subtypes are known to originate from the embryonic caudal ganglionic eminence (CGE), the specific genetic programs that direct their positioning, maturation, and integration into the cortical network have not been elucidated. Here, we report that in mice expression of the transcription factor *Prox1* is selectively maintained in postmitotic CGE-derived cortical interneuron precursors and that loss of *Prox1* impairs the integration of these cells into superficial layers. Moreover, *Prox1* differentially regulates the postnatal maturation of each specific subtype originating from the CGE (RELN, Calb2/VIP, and VIP). Interestingly, *Prox1* promotes the maturation of CGE-derived interneuron subtypes through intrinsic differentiation programs that operate in tandem with extrinsically driven neuronal activity-dependent pathways. Thus *Prox1* represents the first identified transcription factor specifically required for the embryonic and postnatal acquisition of CGE-derived cortical interneuron properties.

Key words: bipolar; mouse genetics; neurogliaform; RELN; transcription; VIP

Significance Statement

Despite the recognition that 30% of GABAergic cortical interneurons originate from the caudal ganglionic eminence (CGE), to date, a specific transcriptional program that selectively regulates the development of these populations has not yet been identified. Moreover, while CGE-derived interneurons display unique patterns of tangential and radial migration and preferentially populate the superficial layers of the cortex, identification of a molecular program that controls these events is lacking.

Here, we demonstrate that the homeodomain transcription factor *Prox1* is expressed in postmitotic CGE-derived cortical interneuron precursors and is maintained into adulthood. We found that *Prox1* function is differentially required during both embryonic and postnatal stages of development to direct the migration, differentiation, circuit integration, and maintenance programs within distinct subtypes of CGE-derived interneurons.

Introduction

Mammalian neocortical circuits are primarily comprised of two interconnected neuronal cell types: excitatory glutamatergic pro-

jection neurons with pyramidal morphologies and a smaller population of inhibitory GABAergic interneurons (~20%), the majority of which project axons locally. GABAergic interneurons can be categorized into numerous diverse subtypes based on their morphology, connectivity, laminar position, molecular expression profile, and intrinsic firing properties (Kubota et al., 1994;

Received March 20, 2015; revised July 31, 2015; accepted Aug. 10, 2015.

Author contributions: G.M. designed research; G.M., A.Y., T.P., T.K., M.M.C., A.L., T.I., and G.F. performed research; G.M., M.N., H.T., Z.J.H., N.H., G.O., and F.M. contributed unpublished reagents/analytic tools; G.M., T.P., T.K., and M.M.C. analyzed data; G.M., R.P.M., and G.F. wrote the paper.

Research in the Fishell lab is supported by National Institutes of Health grants (PPG-NS309889, R01NS039007, R01NS081297, and R01MH071679), the Simons Foundation, and New York State through the NYSTEM initiative. We thank Drs. Stewart Anderson and Sonia Garel for kindly sharing their protocols for embryonic brain slice electroporation and subsequent slice culture. We greatly appreciate the following for kindly sharing their reagents: Dr.

Stewart Anderson (*Nkx2-1BAC-Cre*), Dr. Nicoletta Kessarar (*Lhx6BAC-Cre*), Dr. Ulrich Müller (*Wnt3a-Cre*), Dr. Marc Ekker, and Dr. John Rubenstein (*Dlx6a-Cre*). Finally, we thank the past and present Fishell lab members for their support and constructive comments on this project and Lihong Yin for her technical help.

The authors declare no competing financial interests.

Markram et al., 2004; Kubota et al., 2011; DeFelipe et al., 2013; Fino et al., 2013). It is increasingly becoming evident that this diversity reflects specialized roles for each cortical interneuron subtype in shaping activity within the mature neuronal circuit (Buzsáki et al., 2007; Thomson and Lamy, 2007; Klausberger and Somogyi, 2008; Sohal et al., 2009; Isaacson and Scanziani, 2011; Krook-Magnuson et al., 2012; Kvitsiani et al., 2013; Larkum, 2013). How then does this diversity develop, and what are the mechanisms by which different subtypes of interneurons become integrated into the cortical network?

Work from several research groups has determined the spatiotemporal embryonic origins of GABAergic interneuron diversity (Marín and Rubenstein, 2003; Wonders and Anderson, 2006; Batista-Brito and Fishell, 2009; Gelman and Marín, 2010; Hernández-Miranda et al., 2010; Marín et al., 2010; Le Magueresse and Monyer, 2013; Miyoshi et al., 2013; Kessaris et al., 2014). GABAergic cortical interneurons are not locally generated within the cortical germinal zones; instead they arise from the ventral telencephalon (Anderson et al., 1997), in particular the medial and caudal ganglionic eminences (MGE and CGE; Wichterle et al., 2001; Nery et al., 2002; Xu et al., 2004; Butt et al., 2005; Flames et al., 2007; Fogarty et al., 2007; Miyoshi et al., 2007, 2010; Wonders et al., 2008; Rubin et al., 2010; Inan et al., 2012) as well as the preoptic area (POA; Gelman et al., 2009; Gelman et al., 2011). Cortical interneurons arising from the MGE and CGE give rise to nonoverlapping subtypes that occupy distinct layers of the developing neocortex (Nadarajah et al., 2002; Kriegstein and Noctor, 2004; Tanaka et al., 2006; Fogarty et al., 2007; Métin et al., 2007; Miyoshi et al., 2007, 2010; Li et al., 2008; López-Bendito et al., 2008; Rubin et al., 2010; Sessa et al., 2010; Miyoshi and Fishell, 2011; Marín, 2013). The MGE produces ~70% of the total GABAergic cortical interneuron population, specifically the PV (*Pvalb*, Parvalbumin) and SST (*Sst*, Somatostatin)-expressing classes, which, mirroring pyramidal neurons (Molyneaux et al., 2007; Leone et al., 2008; Rakic, 2009; Franco et al., 2011; Lui et al., 2011; Kwan et al., 2012; Franco and Müller, 2013; Gao et al., 2013), integrate into the cortex in an inside-out pattern (Miller, 1985; Fairén et al., 1986; Miyoshi et al., 2007; Rymar and Sadikot, 2007). In contrast, CGE-derived cortical interneurons comprise ~30% of the total interneuron pool, the vast majority of which express either RELN (*Reln*, Reelin) or VIP (*Vip*, vasoactive intestinal polypeptide), including a subclass that coexpresses CR (*Calb2*, Calretinin; Miyoshi et al., 2010). Unlike MGE lineages, CGE-derived interneurons specifically populate the superficial layers regardless of their birthdate (Miyoshi et al., 2010; Miyoshi and Fishell, 2011). Interestingly, the serotonin receptor *Htr3A* is selectively expressed in CGE-derived interneurons (Lee et al., 2010; Vucurovic et al., 2010) and regulates their embryonic migration (Murthy et al., 2014). Thus there must exist distinct genetic programs that control both the migration and subtype specification of CGE-derived versus MGE-derived cortical interneurons (Kriegstein and Noctor, 2004; Hernández-Miranda et al., 2010; Tanaka and Nakajima, 2012; Marín, 2013; Kessaris et al., 2014).

Here we report that expression of the homeodomain transcription factor *Prox1* is selectively maintained in postmitotic CGE-derived GABAergic cortical interneurons during embry-

onic and postnatal time points and directs the migration and maturation programs of each CGE-derived cortical interneuron subtype.

Materials and Methods

In vivo mouse genetics. All animal handling and experiments were performed in accordance with protocols approved by local Institutional Animal Care and Use Committee of the NYU School of Medicine. The following genetic crosses were generated for our experiments. Total cortical GABAergic populations were visualized with *Dlx5/6-FIpe*; *RCE:FRT* (Miyoshi et al., 2010). MGE-derived GABAergic populations were visualized with *Lhx6BAC-Cre*; *Dlx5/6-FIpe*; *RCE:dual* (Fogarty et al., 2007; Miyoshi et al., 2010). In this cross, to exclude the labeling of blood vessels by the *Lhx6BAC-Cre* driver (repository stock #026555; The Jackson Laboratory), an intersectional strategy was used (Miyoshi and Fishell, 2006; Dymecki and Kim, 2007). The *Dlx6a-Cre* (Monory et al., 2006; repository stock number #008199; The Jackson Laboratory) and *Vip-Cre* (Taniguchi et al., 2011; repository stock number #010908; The Jackson Laboratory) drivers were used in our *Prox1* loss-of-function studies. The *Wnt3a-Cre* driver (Yoshida et al., 2006; Gil-Sanz et al., 2013) was used to verify the *Prox1* expression that occurs transiently within the Cajal–Retzius cells during embryogenesis (data not shown). *Ai9* was used as a red-fluorescent protein (tdTomato) reporter line (repository stock number #007909; The Jackson Laboratory). The *Htr3ABAC-Cre* driver line was generated in a manner similar to the previously generated *Htr3ABAC-EGFP* line (Gong et al., 2003; Lee et al., 2010) and deposited into the GENSAT program. Briefly, the coding region of *Cre* was inserted into ~200 kb of the BAC fragment including the regulatory elements of *Htr3A*. Compound male *Dlx6a-Cre*; *Prox1-F/+* (Harvey et al., 2005) mice were crossed with female *Prox1-C:EGFP/C:EGFP* mice (Iwano et al., 2012) to generate control (*Dlx6a-Cre*; *Prox1-C:EGFP/+*) and *Prox1* loss-of-function (*Dlx6a-Cre*; *Prox1-C:EGFP/F*) experimental animals. This breeding strategy was followed after we observed that the *Dlx6a-Cre* driver caused somatic recombination in the floxed *Prox1* loss-of-function allele (Harvey et al., 2005), most likely during the phase of germline transmission, when these two alleles existed together in females. Genotyping of the two conditional *Prox1* alleles was performed as previously described (Harvey et al., 2005; Iwano et al., 2012). In all of our *Prox1* conditional loss-of-function experiments (*Dlx6a-Cre*, *Htr3ABAC-Cre* and *Vip-Cre*-mediated removal of *Prox1*), we did not observe any obvious difference between the controls and mutants regarding the size of the forebrain as well as the thickness of the cortical layers.

Microarray expression analysis. For the comparison of genes selectively expressed within CGE-derived versus MGE-derived interneuron precursors, we selectively labeled each population with EGFP *in vivo* through the use of *Mash1BAC-CreER*; *RCE:loxP* (Battiste et al., 2007; Miyoshi et al., 2010) and *Nkx2-1BAC-Cre*; *RCE:loxP* (Xu et al., 2008; Sousa et al., 2009) compound transgenic animals, respectively. To generate labeled CGE-derived interneuron precursors within the cortex at E18.5, 4 mg of tamoxifen (in corn oil) was administered by oral gavage to the pregnant dam at E16.5 (Miyoshi et al., 2010). Note that in both genetic labeling strategies, some oligodendrocyte precursors are labeled with EGFP in addition to GABAergic neuronal precursors (Kessaris et al., 2006). By using the fluorescent dissection microscope (Olympus, MVX 10), embryos harboring green brains were selected, brains were dissected out in HBSS solution one by one, meninges were removed, and each pair of cortices was dissected out and stored in a tube with 200 μ l of HBSS solution and kept on ice until the dissection was complete for the entire litter. During this step, a small piece of the embryonic brainstem was also collected in numbered tubes for genotyping. Later, HBSS was removed and 20 μ l of DNase I (2000 U/ml in HBSS; Worthington) and 200 μ l of Papain (20 U/ml in HBSS; Worthington) solution were immediately added. By gentle pipetting (typically approximately 10–15 times) with a 200 μ l filter tip pipette, cortices were broken into small pieces. After 20 min of incubation at 37°C, 750 μ l of 1% (v/v) normal horse serum (Gibco) in ice-cold HBSS and 75 μ l of DNase I (2000 U/ml in HBSS) were added. After gently inverting the tubes a couple of times, tubes were

Table 1. Genes enriched in CGE-derived versus MGE-derived interneurons at E18.5

Symbol: Name	Fold change
CCND2: cyclin D2	107.68
MK167: antigen identified by monoclonal antibody Ki-67	67.082
TOP2A: topoisomerase (DNA) II α 170 kDa	64.226
MEIS2: Meis homeobox 2	60.951
RRM2: ribonucleotide reductase M2	54.829
SYNPR: synaptopodin	53.649
WNT5A: wingless-type MMTV integration site family, member 5A	43.522
CENPF: centromere protein F, 350/400 kDa	42.989
CEP55: centrosomal protein 55 kDa	39.435
Ccnb1/Gm5593: cyclin B1	37.666
CDC45: cell division cycle associated 5	35.871
PBK: PDZ binding kinase	35.556
EZR: ezrin	33.941
KIF2C: kinesin family member 2C	31.704
VIM: vimentin	31.315
NUSAP1: nucleolar and spindle associated protein 1	28.928
MELK: maternal embryonic leucine zipper kinase	27.681
EMP1: epithelial membrane protein 1	23.414
CENPA: centromere protein A	23.144
KIF22: kinesin family member 22	23.11
PAX6: paired box 6	23.073
CENPE: centromere protein E, 312 kDa	22.218
NR2F2: nuclear receptor subfamily 2, group F, member 2	21.87
CKS2: CDC28 protein kinase regulatory subunit 2	21.21
SPAG5: sperm associated antigen 5	21.161
ECT2: epithelial cell transforming sequence 2 oncogene	21.113
RWDD3: RWD domain containing 3	20.515
CDK1: cyclin-dependent kinase 1	20.515
TMEM123: transmembrane protein 123	20.48
ASPM: asp (abnormal spindle) homolog, microcephaly associated (<i>Drosophila</i>)	20.245
BIRC5: baculoviral IAP repeat containing 5	19.555
DTL: denticleless E3 ubiquitin protein ligase homolog (<i>Drosophila</i>)	19.304
BRCA1: breast cancer 1, early onset	17.891
ANLN: anillin, actin binding protein	16.842
SHCBP1: SHC SH2-domain binding protein 1	16.766
MIS18BP1: MIS18 binding protein 1	16.608
EGLN3: egl nine homolog 3 (<i>Caenorhabditis elegans</i>)	15.965
CCNA2: cyclin A2	15.743
TPX2: TPX2, microtubule-associated, homolog (<i>Xenopus laevis</i>)	15.409
CDC20: cell division cycle 20	15.237
DEPDC1: DEP domain containing 1	15.082
CXCL14: chemokine (C-X-C motif) ligand 14	14.875
AURKB: aurora kinase B	14.806
MCM2: minichromosome maintenance complex component 2	14.643
KIF18A: kinesin family member 18A	14.561
KIF20A: kinesin family member 20A	14.086
GRB10: growth factor receptor-bound protein 10	13.737
MCM3: minichromosome maintenance complex component 3	13.63
LRR1: leucine-rich repeat protein 1	13.588
BUB1: BUB1 mitotic checkpoint serine/threonine kinase	13.53
RACGAP1: Rac GTPase activating protein 1	13.465
HBA1/HBA2: hemoglobin, α -1	13.359
DNA2: DNA replication helicase 2 homolog (yeast)	13.219
KIF11: kinesin family member 11	13.138
RLBP1: retinaldehyde binding protein 1	13.003
PLK4: polo-like kinase 4	12.999
NCAPG: non-SMC condensin I complex, subunit G	12.724
PSRC1: proline/serine-rich coiled-coil 1	12.714
CCNB2: cyclin B2	12.388
PROX1: prospero homeobox 1	12.378
STIL: SCL/TAL1 interrupting locus	12.191
PRC1: protein regulator of cytokinesis 1	12.157
HTR3A: 5-hydroxytryptamine (serotonin) receptor 3A, ionotropic	11.839
CDC109B: coiled-coil domain containing 109B	11.835

(Table Continues)

Table 1. Continued

Symbol: Name	Fold change
CRYAB: crystallin, α -B	11.75
GMNN: geminin, DNA replication inhibitor	11.692
TTK: TTK protein kinase	11.145
SPC25: SPC25, NDC80 kinetochore complex component, homolog	11.138
TUBA1C: tubulin, α -1c	11.057
TCF19: transcription factor 19	10.957
CDC6: cell division cycle 6	10.9
NEDD9: neural precursor cell expressed, developmentally downregulated 9	10.727
UHRF1: ubiquitin-like with PHD and ring finger domains 1	10.651
SORCS3: sortilin-related VPS10 domain containing receptor 3	10.229
SPON1: spondin 1, extracellular matrix protein	10.21
HMGB2: high mobility group box 2	10.171
RAD51AP1: RAD51 associated protein 1	10.081
RAI14: retinoic acid induced 14	10.036

centrifuged for 3 min at 0.3 relative centrifugal force (rcf), the supernatant was discarded, 500 μ l of ice-cold HBSS (containing 5 μ l of DNase I) was added, and the cell pellet was resuspended by gentle pipetting using a 1000 μ l filter tip pipette. These cells were subjected to FACS (MoFlo; Beckman Coulter), and EGFP-positive cells were collected into numbered tubes containing 500 μ l of ice-cold HBSS. Cell numbers were typically between 10,000–20,000 and 20,000–30,000 cells per brain for CGE-derived and MGE-derived populations, respectively. These tubes were then centrifuged for 5 min at 0.3 rcf, supernatant was discarded, and tubes were snap frozen in liquid nitrogen and stored at -80°C until mRNA extraction and subsequent labeling. RNA extraction, labeling, and subsequent microarray expression analyses using Affymetrix Gene Chips (Mouse 430A.2, which contains 45,000 probe sets covering over 39,000 transcripts) were performed at the Genomic Core Laboratory at the Memorial Sloan Kettering Center. Analyses of the changes in gene expression profiles in the conditional *Prox1* loss-of-function experiments were performed in a very similar manner by comparing the mRNA transcriptomes of the EGFP-labeled cells purified from the E18.5 cortices of control heterozygous and *Prox1* loss-of-function animals (*Dlx6a-Cre; Prox1-C:EGFP/+* and */F*).

The raw probe-level expression measurements were obtained from the Affymetrix CEL files. Analysis of microarray data was performed using Ingenuity iReport. Probe set intensities were summarized and normalized using RMA, and significant differential expression was determined by a moderated *t* test (LIMMA) using an FDR-adjusted *p* value cutoff (*Q* value) of 0.05 and a fold change cutoff of 1.5. For the gene expression comparison of CGE-derived versus MGE-derived interneurons, we acquired 723 significantly differentially expressed probe sets resulting in 567 genes with 382 CGE-enriched and 185 MGE-enriched genes (Tables 1 and 2). For the analysis of *Prox1* loss-of-function, we acquired 93 probe sets resulting in 46 upregulated and 33 downregulated genes upon *Prox1* loss-of-function. Since we analyzed three male and three female samples by chance for the comparison of control and *Prox1* loss-of-function, respectively, we found several gender-specific genes with significant and large changes (Table 3).

CGE cell transplantation into the postnatal cortex. CGE tissues were dissected from control and *Prox1* loss-of-function (*Dlx6a-Cre; Prox1-C:EGFP/+* and */F*) mutants at E14.5 and cells were dissociated and stored in individual tubes on ice. These cell suspensions were prepared in a manner identical to that described above for FACS purification of cells in our microarray analysis. However, the procedure before the cell-sorting step was changed: the cell pellets were resuspended into 200 μ l of ice-cold NB/B27 tissue culture medium containing 5 μ l of DNase I, instead of HBSS solution. The dissociated CGE including EGFP-labeled cells was typically between 1500 and 3000 cells/ μ l in a total of 200 μ l. Cell concentration was adjusted to \sim 5000 cells/ μ l by removing the supernatant after centrifuging the tubes, and cells were kept on ice typically \sim 1–4 h before the subsequent transplantation step.

Cell transplantation into P3 pup cortices was performed following the protocol of the Anderson lab as previously described (Inan et al., 2012).

Table 2. Genes enriched in MGE-derived versus CGE-derived interneurons at E18.5

Symbol: Name	Fold change
PALD1: phosphatase domain containing, paladin 1	56.966
GRIA1: glutamate receptor, ionotropic, AMPA 1	27.832
LHX6: LIM homeobox 6	22.68
C8orf4: chromosome 8 open reading frame 4	18.462
NXPH1: neuroligin 1	14.768
ID3: inhibitor of DNA binding 3, dominant negative helix-loop-helix protein	11.804
CXCR7: chemokine (C-X-C motif) receptor 7	11.699
MEF2C: myocyte enhancer factor 2C	11.461
MAFB: v-maf musculoaponeurotic fibrosarcoma oncogene homolog B (avian)	11.068
GUCY1A3: guanylate cyclase 1, soluble, α -3	10.147
CUX2: cut-like homeobox 2	9.613
RPH3A: rabphilin 3A homolog (mouse)	8.384
NPY: neuropeptide Y	8.362
MAN1A1: mannosidase, α , class 1A, member 1	8.053
THBS1: thrombospondin 1	8.04
TGFB2: transforming growth factor, β 2	7.935
KLF5: Kruppel-like factor 5 (intestinal)	7.882
HNMT: histamine N-methyltransferase	7.848
IGFBP4: insulin-like growth factor binding protein 4	7.575
RPP25: ribonuclease P/MRP 25 kDa subunit	7.443
PPARGC1A: peroxisome proliferator-activated receptor γ , coactivator 1 α	7.198
NID2: nidogen 2 (osteonidogen)	7.115
CBFA2T3: core-binding factor, runt domain, α -subunit 2; translocated to, 3	7.053
DMD: dystrophin	6.861
PLXDC2: plexin domain containing 2	6.792
C1QTNF4: C1q and tumor necrosis factor-related protein 4	6.643
SCN1A: sodium channel, voltage-gated, type I, α -subunit	6.414
RBFOX1: RNA binding protein, fox-1 homolog (<i>C. elegans</i>) 1	6.172
GALC: galactosylceramidase	6.013
APC: adenomatous polyposis coli	5.977
DGKG: diacylglycerol kinase, γ 90 kDa	5.965
KCNK2: potassium channel, subfamily K, member 2	5.918
SST: somatostatin	5.719
Gm16489: predicted gene 16489	5.705
RUFY2: RUN and FYVE domain containing 2	5.469
TGFB3: transforming growth factor, β 3	5.267
SEMA3A: sema domain, immunoglobulin domain (Ig), short basic domain, secreted, (semaphorin) 3A	5.218
SMARCA2: SWI/SNF-related, matrix-associated, actin-dependent regulator of chromatin, subfamily a, member 2	5.136
PHLDA1: pleckstrin homology-like domain, family A, member 1	5.095
NOX4: NADPH oxidase 4	5.046
MMP2: matrix metalloproteinase 2 (gelatinase A, 72 kDa gelatinase, 72 kDa type IV collagenase)	5.013
EPB41L4A: erythrocyte membrane protein band 4.1 like 4A	4.869
SLA: Src-like-adaptor	4.596
CDH9: cadherin 9, type 2 (T1-cadherin)	4.587
CACNA2D2: calcium channel, voltage-dependent, α 2/ δ -subunit 2	4.552
DPF1: D4, zinc and double PHD fingers family 1	4.485
PKP4: plakophilin 4	4.453
Ptprd: protein tyrosine phosphatase, receptor type, D	4.411
Pisd-ps3: phosphatidylserine decarboxylase, pseudogene 3	4.404
RUNX1T1: runt-related transcription factor 1; translocated to, 1 (cyclin D-related)	4.39
NETO1: neuropilin (NRP) and tolloid (TLL)-like 1	4.39
PCMTD1: protein-L-isoaspartate (β -aspartate) O-methyltransferase domain containing 1	4.323
NPNT: nephronectin	4.183
MYH7: myosin, heavy chain 7, cardiac muscle, β	4.141
SCUBE1: signal peptide, CUB domain, EGF-like 1	4.083
ARHGAP20: Rho GTPase activating protein 20	4.016
DCX: doublecortin	4
KCNMB2: potassium large conductance calcium-activated channel, subfamily M, β member 2	3.909

(Table Continues)

Table 2. Continued

Symbol: Name	Fold change
SOX6: SRY (sex determining region Y)-box 6	3.891
SATB1: SATB homeobox 1	3.882
CDK20: cyclin-dependent kinase 20	3.818
SPATS2L: spermatogenesis associated, serine-rich 2-like	3.802
KIF2A: kinesin heavy chain member 2A	3.753
PDE2A: phosphodiesterase 2A, cGMP-stimulated	3.641
Fhod3: formin homology 2 domain containing 3	3.514
KCTD12: potassium channel tetramerization domain containing 12	3.479
SERPINI1: serpin peptidase inhibitor, clade I (neuroserpin), member 1	3.476
FAM19A5: family with sequence similarity 19 (chemokine (C-C motif)-like), member A5	3.476
ALK: anaplastic lymphoma receptor tyrosine kinase	3.385
FURIN: furin (paired basic amino acid cleaving enzyme)	3.371
ARL4D: ADP-ribosylation factor-like 4D	3.32
FUT9: fucosyltransferase 9 (α (1,3) fucosyltransferase)	3.304
PTPRT: protein tyrosine phosphatase, receptor type, T	3.295
RYR2: ryanodine receptor 2 (cardiac)	3.28
MTM1: myotubularin 1	3.259
SKI: v-ski sarcoma viral oncogene homolog (avian)	3.232
CNTNAP2: contactin associated protein-like 2	3.223
DUSP26: dual specificity phosphatase 26 (putative)	3.206
TENM2: teneurin transmembrane protein 2	3.185
MAP4K5: mitogen-activated protein kinase kinase kinase kinase 5	3.178
ATP1B1: ATPase, Na ⁺ /K ⁺ transporting, β 1 polypeptide	3.15
CDH13: cadherin 13, H-cadherin (heart)	3.139
VSTM2B: V-set and transmembrane domain containing 2B	3.098
SPTBN1: spectrin, β , nonerythrocytic 1	3.082
EPHA5: EPH receptor A5	3.056
Pcdhb21: protocadherin β 21	3.042
SLC22A3: solute carrier family 22 (extraneuronal monoamine transporter), member 3	3.041
CNTNAP4: contactin associated protein-like 4	3.04
ATP1A3: ATPase, Na ⁺ /K ⁺ transporting, α 3 polypeptide	3.034

Briefly, P3 pups were anesthetized on ice for 5 min and stabilized on a Styrofoam platform. Approximately 5 μ l of CGE cells was loaded into a capillary electrode prefilled with mineral oil and loaded into an oocyte nanoinjector (Drummond). Each pup received two injections bilaterally into the somatosensory cortex of each hemisphere at a location of 1 mm lateral to the midline and 1 and 2 mm rostral of the interaural line, at a depth of 1 mm. Each injection site consisted of ~60 mini injections of 69 nl of cell suspension (total of ~4 μ l). After injections, the pup was labeled and placed back in the nest, and analyses were performed at the age of P21.

Tissue preparation and immunohistochemistry. Embryos were dissected out, and transcardiac perfusion was performed with cold 4% formaldehyde/PBS solution (w/v). Brain dissection was performed in PBS in a Petri dish, and brains were subsequently placed into 4% formaldehyde/PBS solution on ice. Brains were postfixed according to the developmental stages (E14.5: 20 min, E16.5: 40 min, E18.5 onward: 60 min) and, following a brief rinse in PBS, were placed into cold 25% sucrose/PBS (w/v) solution for cryoprotection until they sunk to the bottom. Exceptions were E10.5 embryos: after peeling the thin skin layer of the head, the entire bodies were placed into 4% formaldehyde/PBS solution on ice for 20 min. Later brains or embryos were placed into OCT compound (Sakura Finetek) and kept at -80°C . Cryosections were prepared at 12 μm thickness and collected on glass slides (Fisher), and, after ~1 h of drying, the sections were stored at -80°C . For the morphological analysis of *Prox1* loss-of-function cells, 100 μm cryosections were immediately placed into PBS solution and stored at 4°C until further analysis.

Immunohistochemistry was performed as previously described (Miyoshi and Fishell, 2012). All incubations were performed in PBS containing 1.5% normal donkey serum (Jackson ImmunoResearch; v/v) and 0.1% Triton X-100 (v/v; DST solution). Sections were rinsed three times in PBS to remove the residual OCT, followed by nonspecific antibody

Table 3. Gene expression comparison between *Prox1* heterozygous versus null in CGE-derived interneuron precursors within the E18.5 cortex

Symbol: Name	Fold change
Genes upregulated in CGE-derived <i>Prox1</i> loss-of-function cells in the E18.5 cortex	
XIST: X inactive-specific transcript (nonprotein coding)	376.517
SLN: sarcolipin	5.321
SFRP2: secreted frizzled-related protein 2	4.251
SCN1A: sodium channel, voltage-gated, type I, α -subunit	3.998
C1QTNF1: C1q and tumor necrosis factor-related protein 1	3.558
NTNG1: netrin G1	3.009
PROX1: prospero homeobox 1	2.717
DLK1: δ -like 1 homolog (<i>Drosophila</i>)	2.709
MSRB2: methionine sulfoxide reductase B2	2.384
SVIL: supervillin	2.377
DUSP26: dual specificity phosphatase 26 (putative)	2.287
TGFB1: transforming growth factor, β -induced, 68 kDa	2.15
Etl4: enhancer trap locus 4/KIAA1217	2.142
GABRA2: GABA A receptor, α 2	2.14
DBC1: deleted in bladder cancer 1	2.083
FGA: fibrinogen α chain	2.034
Rnd3: Rho family GTPase 3	1.991
SEZ6L: seizure-related 6 homolog (mouse)-like	1.958
HCN1: hyperpolarization activated cyclic nucleotide-gated potassium channel 1	1.926
PAG1: phosphoprotein associated with glycosphingolipid microdomains 1	1.915
ligp1: interferon inducible GTPase 1	1.896
MPDZ: multiple PDZ domain protein	1.893
DNAH8: dynein, axonemal, heavy chain 8	1.886
SLC4A4: solute carrier family 4, sodium bicarbonate cotransporter, member 4	1.86
NRP2: neuropilin 2	1.783
RNGTT: RNA guanylyltransferase and 5'-phosphatase	1.782
APCDD1: adenomatosis polyposis coli downregulated 1	1.756
TMEM176B: transmembrane protein 176B	1.745
SHISA2: shisa homolog 2 (<i>Xenopus laevis</i>)	1.706
PLAGL1: pleomorphic adenoma gene-like 1	1.694
CUX2: cut-like homeobox 2	1.689
CALB1: calbindin 1, 28 kDa	1.676
CACHD1: cache domain containing 1	1.657
SPC25: SPC25, NDC80 kinetochore complex component, homolog (<i>S. cerevisiae</i>)	1.653
ENPP3: ectonucleotide pyrophosphatase/phosphodiesterase 3	1.65
DTNA: dystrobrevin, α	1.634
HNMT: histamine N-methyltransferase	1.628
FGF12: fibroblast growth factor 12	1.625
SCHIP1: schwannomin interacting protein 1	1.586
NPPA: natriuretic peptide A	1.576
EPB41L4A: erythrocyte membrane protein band 4.1 like 4A	1.565
CST3: cystatin C	1.546
TRIM25: tripartite motif containing 25	1.544
ZFX3: zinc finger homeobox 3	1.541
NPTX2: neuronal pentraxin II	1.537
SEMA4A: semaphorin 4A	1.532
SLC6A15: solute carrier family 6 (neutral amino acid transporter), member 15	1.529
Genes downregulated in CGE-derived <i>Prox1</i> loss-of-function cells in the E18.5 cortex	
Ddx3y: DEAD (Asp-Glu-Ala-Asp) box polypeptide 3, Y-linked	67.225
EIF2S3: eukaryotic translation initiation factor 2, subunit 3 γ, 52 kDa	51.606
KDM5D: lysine (K)-specific demethylase 5D	20.671
VIP: vasoactive intestinal peptide	14.152
Uty: ubiquitously transcribed tetratricopeptide repeat gene, Y chromosome	5.435
TRIL: TLR4 interactor with leucine-rich repeats	4.79
CCK: cholecystokinin	3.224
RSP02: R-spondin 2	2.076

(Table Continues)

Table 3. Continued

Symbol: Name	Fold change
FGFR1: fibroblast growth factor receptor 1	1.908
CRABP1: cellular retinoic acid binding protein 1	1.858
TMEFF2: transmembrane protein with EGF-like and two follistatin-like domains 2	1.814
CALB2: calbindin 2	1.787
SPEG: SPEG complex locus	1.776
ID4: inhibitor of DNA binding 4, dominant negative helix-loop-helix protein	1.762
ROBO1: roundabout, axon guidance receptor, homolog 1 (<i>Drosophila</i>)	1.746
CRIM1: cysteine-rich transmembrane BMP regulator 1 (chordin-like)	1.745
MYO1B: myosin IB	1.686
NAV2: neuron navigator 2	1.671
CPNE2: copine II	1.671
PTPRE: protein tyrosine phosphatase, receptor type, E	1.665
CACNA1G: calcium channel, voltage-dependent, T type, α -1G-subunit	1.618
GNAI1: guanine nucleotide binding protein (G-protein), α -inhibiting activity polypeptide 1	1.592
CHST15: carbohydrate (<i>N</i> -acetylgalactosamine 4-sulfate 6- <i>O</i>) sulfotransferase 15	1.585
FAM134B: family with sequence similarity 134, member B	1.579
BCKDHB: branched chain keto acid dehydrogenase E1, β -polypeptide	1.567
Rcan2: regulator of calcineurin 2	1.555
NRIP3: nuclear receptor interacting protein 3	1.545
ZDHC2: zinc finger, DHC-type containing 2	1.542
IL-18: interleukin 18 (interferon- γ -inducing factor)	1.536
CCRN4L: CCR4 carbon catabolite repression 4-like (<i>S. cerevisiae</i>)	1.535
WWC1: WW and C2 domain containing 1	1.528
PRKC: protein kinase C, ϵ	1.519
HSD11B1: hydroxysteroid (11- β) dehydrogenase 1	1.51

We FACS purified EGFP-labeled cells from the E18.5 cortices of control and *Prox1* loss-of-function animals (*Dlx6a-Cre; Prox1-CreGFP/+* and */-*) and subsequently performed a microarray expression analysis. Genes are shown upregulated and downregulated in cells lacking *Prox1*, respectively. Genes are shown for FDR-adjusted *p*-value (<0.05) and fold change (>1.5). Note that the values of gender-linked genes are indicated with boldface as male–female split happened by chance across control and *Prox1* loss-of-function brains.

blocking, which was performed in DST solution at room temperature for 30–60 min. Primary antibody incubation was subsequently performed overnight at 4°C. Primary antibody was added to the DST solution at the following concentrations: rabbit anti-GFP (1:2000; Invitrogen, #A11122), rat anti-GFP #GF090R (1:2000; Nacalai Tesque, #04404-84), chicken anti-GFP (1:2000; Abcam, #ab13970), rat anti-RFP #5F8 (1:2000; Allele Biotechnology, #ACT-CM-MRRFP10), rabbit anti-RFP (1:2000; Clontech, #632496), goat anti-*Prox1* N terminus (1:1000; R&D Systems, #AF2727), rabbit anti-*Prox1* C terminus (1:1000; Abcam, #ab11941-100), mouse anti-Nkx2-1 #8G7G3/1 (1:1000; Progen, #16108), rabbit anti-Nkx2-1 #EP1584Y (1:2000; Abcam, #ab76013), goat anti-Sp8 (Santa Cruz Biotechnology, #sc-104661), mouse anti-CoupTFII #7147 (Perseus Proteomics, #PP-H7147-00), mouse anti-RELN #CR-50 (1:1000; MBL, #D223-3), goat anti-RELN (1:1000; R&D Systems, #AF3820), mouse anti-PV #PARV-19 (1:2000; Sigma, #P3088), rat anti-SST #YC7 (1:1000; Millipore Bioscience Research Reagents, #MAB354), rabbit anti-SST (1:1000; Millipore Bioscience Research Reagents, #AB5494), rabbit anti-VIP (1:1000; ImmunoStar, #20077), mouse anti-Calretinin (1:1500; Millipore Bioscience Research Reagents, #MAB1568), and rabbit anti-Calretinin (1:1500; Millipore Bioscience Research Reagents, #AB5054). Secondary antibodies conjugated with Alexa Fluor dyes 488 and 594 (Invitrogen; 1:2000 dilutions) or DyLight 649 (Jackson ImmunoResearch; 1:1000 dilutions) raised in donkey were chosen for visualizing the primary antibody staining. To visualize the cell nuclei and the laminar structure of the developing neocortex, DAPI (Sigma; 1 $\mu\text{g}/\mu\text{l}$ in PBS and filtered) was added on slides at the end of the immunohistochemistry procedure for 10–15 min. Slides were rinsed a couple of times in PBS and then mounted in Fluoromount G (Southern Biotech). Fluorescent images were captured using a cooled-CCD camera (Princeton Scientific Instruments) using MetaMorph software (Universal Imaging).

To better visualize the morphologies of EGFP-labeled interneurons with immunohistochemistry, 100 μm cryosections were generated and, by using the confocal microscope LSM 510 (Carl Zeiss), images were captured every 4 μm of optical distance and a stacked view was made typically by combining three to four images.

After the electrophysiological recordings, *post hoc* immunohistochemistry was performed on 250- μm -thick vibratome sections. Sections were fixed for 2 h on ice with 4% formaldehyde containing PBS, and after 30 min of multiple PBS rinses, incubated for two or three overnights at 4°C with selected antibodies. We found that the fixation time is critical, especially for VIP immunohistochemistry. Sections were washed in PBS typically from the morning to the late afternoon and incubated at 4°C overnight with donkey secondary antibodies (The Jackson Laboratory) together with Alexa 488-conjugated streptavidin (1:1000; Invitrogen, #S-11223). Later, sections were rinsed with PBS and submerged in DAPI solution for 30 min and after multiple washes with PBS mounted and coverslipped on a slide glass with a lid with two layers of electrical tape. See details for the general immunohistochemistry procedure in the above section.

Marker and layer analysis of cortical interneuron distribution. For the P21 analysis of *Dlx6a-Cre* control and *Prox1* loss-of-function interneurons, pictures were taken from six representative hemispheric fields per brain for SST/RELN/EGFP/DAPI and CR/VIP/EGFP/DAPI-labeled sections. Image acquisition was performed in the somatosensory barrel field with a 10 \times lens and two pictures were combined to cover the cortical layers from I to VI. By using Adobe Photoshop, DAPI was placed in a different picture layer, layer borders of the cortex were drawn using the pen tool based on the DAPI signal, and then the DAPI picture layer was made invisible. The cell numbers were determined for each specific labeling (e.g., SST-/RELN+/EGFP+, SST+/RELN+/EGFP-) in cortical layers I, II/III, IV, V, and VI. At the end of the cell counting, two lines were drawn following the superficial edge of the cortex and the bottom of layer VI and total pixel numbers between these two lines were analyzed and then converted to the surface area for 2.4 M pixels = 1 mm². Marker profiles (cell numbers for each layer) were converted to cell density (cells/1 mm²) for each section, and the values from the six fields from each brain sample were averaged per brain and final results were shown as the average \pm SEM from three brains for each marker analysis. For the analysis of PV expression, since we found no overlap between PV and EGFP in both control and *Prox1* loss-of-function brains, we simply counted the total numbers of PV-positive cells within the six fields, calculated the cell density, and averaged for three brains. For the P7 analysis, the profile for CR/VIP/EGFP/DAPI was analyzed. Similar analyses were performed for the images obtained from the experiments using the *Htr3ABAC-Cre* and *Vip-Cre* driver lines to remove *Prox1*.

Electrophysiology and data analysis. Whole-cell patch-clamp electrophysiological recordings were performed on randomly selected cells located in neocortical layers I–III labeled with EGFP in acute brain slices prepared from control and *Prox1* loss-of-function (*Dlx6a-Cre*; *Prox1-C:EGFP/+* and */F*) P16–P20 animals. Briefly, animals were decapitated and the brain was dissected out and transferred to physiological Ringer's solution (ACSF) in 4°C with the following composition (mM): 125 NaCl, 2.5 KCl, 25 NaHCO₃, 1.25 NaH₂PO₄, 1 MgCl₂, 2 CaCl₂, and 20 glucose. The brain was then glue fixed to a stage and 250 μm slices were cut using a vibratome (Vibratome 3000 EP). The slices were allowed to recover in recording ACSF at room temperature for at least 45 min before recording. Acute slices were then placed in a recording chamber mounted on the stage of an upright microscope (Axio Scope; Zeiss) equipped with immersion differential interference contrast objectives (5 \times and 40 \times) coupled to an infrared camera system (Zeiss), perfused at a rate of 1–2 ml/min with oxygenated recording ACSF, and maintained at a temperature of 31°C. An EGFP filter was used to visualize the interneurons in epifluorescence.

Patch electrodes were made from borosilicate glass (Harvard Apparatus) and had a resistance of 4–8 M Ω . For both intrinsic electrophysiological properties and sEPSC recordings the patch pipettes were filled with a solution containing the following (in mM): 128 K-gluconate, 4 NaCl, 0.3 Na-GTP, 5 Mg-ATP, 0.0001 CaCl₂, and 10 HEPES.

Experiments were performed in current-clamp and voltage-clamp mode using the Axopatch 200B amplifier (Molecular Devices). sEPSCs were recorded at $V_h = -70$ mV with a sampling rate of 10 kHz and were filtered on-line at 3 kHz. The recorded sEPSCs were analyzed using Mini Analysis software (Synaptosoft). The synaptic values were obtained for the average trace after visual inspection of individual events. The decay time was calculated by fitting the average trace with a single exponential. Access resistance was always monitored to ensure the stability of recording conditions. Cells were only accepted for analysis if the initial series resistance was <40 M Ω and did not change by >20% throughout the recording period. No compensation was made for access resistance and no correction was made for the junction potential between the pipette and the ACSF.

Passive and active membrane properties were recorded in current-clamp mode by applying a series of subthreshold and suprathreshold current steps and the analysis was done in Clampfit. The resting membrane potential (V_{rest}) was ascertained in current-clamp right after rupturing the patch by applying zero current. All values presented are average \pm SEM.

Results

Within cortical interneuron lineages, *Prox1* expression is selectively maintained in CGE-derived subtypes

During the development of GABAergic cortical interneuron populations, a sequential transcriptional cascade of *Nkx2-1–Lhx6–Sox6/SatB1* expression has been established as critical for the specification, migration, and maturation of MGE-derived lineages (Sussel et al., 1999; Liodis et al., 2007; Butt et al., 2008; Du et al., 2008; Zhao et al., 2008; Azim et al., 2009; Batista-Brito et al., 2009; Balamotis et al., 2012; Close et al., 2012; Denaxa et al., 2012; Narboux-Nême et al., 2012). However, aside from transcription factors, *Dlx*, *Arx*, and *CoupTF*, which participate in the early development of both MGE and CGE cortical interneuron subtypes (Cobos et al., 2005b; Colasante et al., 2008; Friocourt et al., 2008; Kanatani et al., 2008; Lodato et al., 2011), a distinct genetic cascade that regulates CGE-derived cortical interneuron development has not yet been characterized.

To identify genes specifically enriched in CGE-derived interneurons, we performed a comparative gene expression analysis using oligonucleotide microarrays on RNA extracted from EGFP-labeled interneuron precursors derived from the CGE or the MGE that were FACS purified from the E18.5 cortex (Tables 1 and 2). Selective labeling of CGE-derived or MGE-derived cortical interneuron precursors was achieved through use of the *Mash1BAC-CreER* (Battiste et al., 2007; Miyoshi et al., 2010) or *Nkx2-1BAC-Cre* (Xu et al., 2008) driver lines, respectively. This analysis revealed that the expression of *Prox1* is highly enriched ($\times 12.4$; Table 1) within CGE-derived versus MGE-derived cortical interneurons at E18.5. *Prox1* is a mammalian homolog of *Prospero*, which determines cell fate through its asymmetric localization in dividing neuroblasts within the fruit fly larva (Choksi et al., 2006; Doe, 2008) as well as in photoreceptor progenitors (Cook et al., 2003). Similarly, in the hippocampus, *Prox1* has been shown to play important roles in cell proliferation (Kaltezioti et al., 2010; Lavado et al., 2010) and fate determination (Iwano et al., 2012). Since *Prox1* is further demonstrated to be essential for the development of horizontal cells, which are the interneurons of the retinal circuit (Dyer et al., 2003), we hypothesized that it plays important roles in the GABAergic local interneurons within the cerebral cortex.

We next characterized the expression of *Prox1* within the developing telencephalon using immunohistochemistry. At E10.5, *Prox1* is expressed in the subventricular zones of the MGE (defined by *Nkx2-1* expression), lateral GE (LGE), and CGE (Fig. 1A,B; Lavado and Oliver, 2007). This is consistent with the pre-

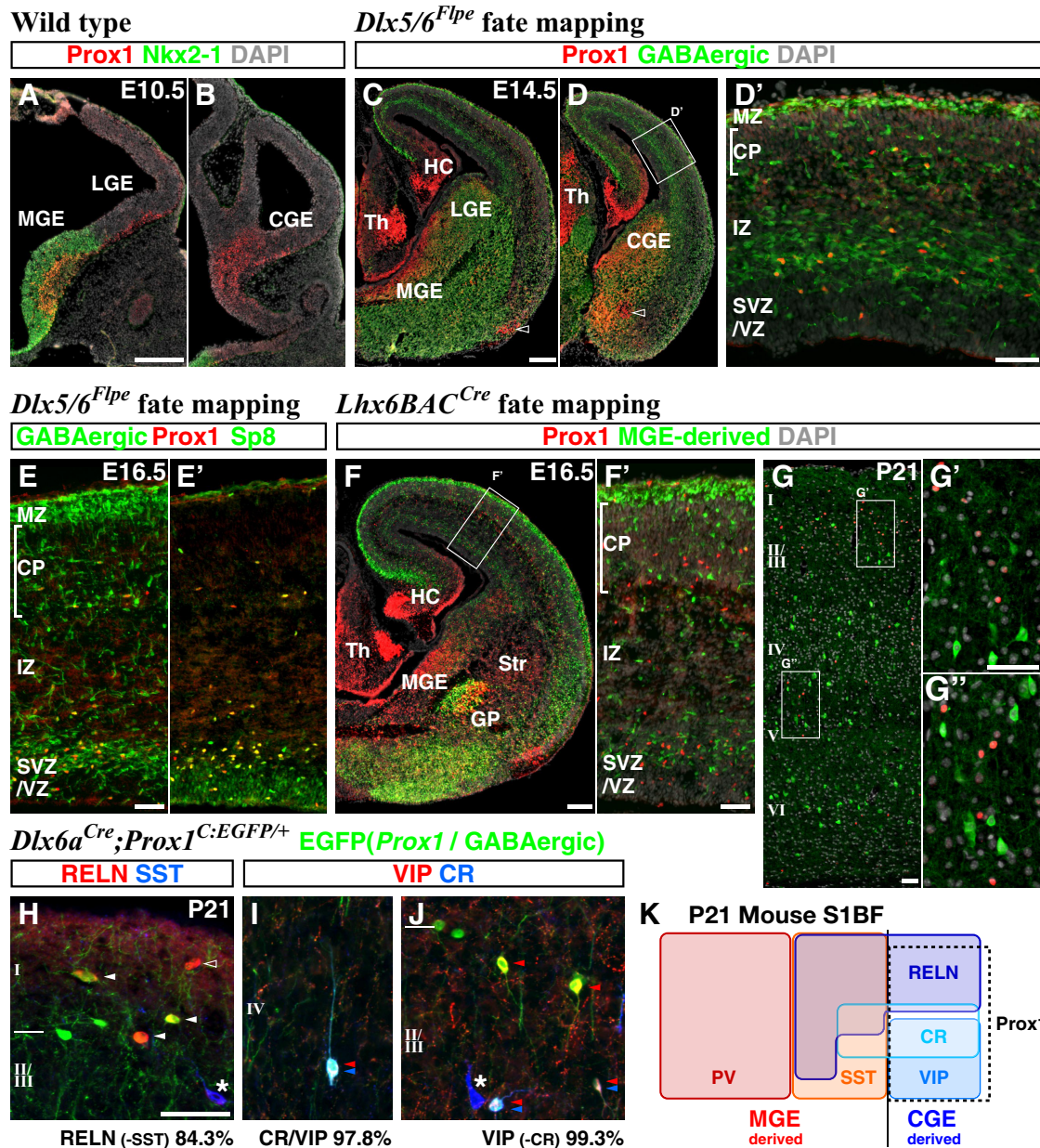


Figure 1. CGE-derived but not MGE-derived GABAergic cortical interneurons maintain expression of the transcription factor *Prox1* during their development. **A, B**, Immunohistochemistry for *Prox1* reveals expression within the SVZs of the ventral eminences (MGE, LGE, and CGE) as early as E10.5. Expression of *Nkx2-1* largely demarcates the MGE domain. DAPI nuclear counterstain is shown in white. **C, D**, GABAergic neuronal precursors in the forebrain are labeled by EGFP through combinatorial use of a *Dlx5/6-Flpe* driver and an *RCE:FRT* reporter at E14.5. High levels of *Prox1* expression are found in the SVZs of the MGE and CGE. Some non-GABAergic populations in the ventral forebrain also express *Prox1* (open arrowheads). **D'**, A higher magnification picture of the neocortex in **D** is shown. Most *Prox1*-expressing cells are found to be GABAergic in the cortical plate (CP), intermediate zone (IZ), and subventricular/ventricular zones (SVZ/VZ). Non-GABAergic *Prox1*-expressing cells (red without green) within the marginal zone (MZ) are Cajal–Retzius cells and *Prox1* expression within this population shuts off by E18.5 (confirmed by *Wnt3a-Cre* driver fate mapping; data not shown). **E, E'**, At E16.5, *Prox1* expression is largely confined to GABAergic neuronal precursors within the cortex (**E**) and overlaps with *Sp8* (**E'**). **F, G**, MGE-derived GABAergic populations are labeled with EGFP in *Lhx6BAC-Cre; Dlx5/6-Flpe; RCE:dual* animals. MGE-derived cortical interneuron precursors at E16.5 do not express *Prox1* (**F, F'**). At P21, *Prox1* remains absent from MGE-derived interneurons (**G–G'**). **H–J**, Analysis of *Prox1* expression in specific CGE-derived cortical interneuron subtypes in *Dlx6a-Cre; Prox1-C:EGFP/+* P21 brains. **H**, RELN-expressing interneurons that are negative for SST originate from the embryonic CGE and *Prox1* expression (EGFP) are observed in 84.3% of this population albeit at variable levels (arrowheads; open arrowhead indicates *Prox1*-negative RELN-positive cell). SST-positive cells do not express *Prox1* (asterisk). **I, J**, The majority of CR(Calb2)/VIP (double arrowheads) and VIP-single (single arrowhead) populations express *Prox1*. Most CR-positive cells lacking VIP are MGE derived (**K**) and do not express *Prox1* (asterisk). **K**, A schematic correlating the molecular expression and the embryonic origin of GABAergic interneurons within the P21 mouse somatosensory barrel cortex (S1BF; adapted from Miyoshi et al., 2010). *Prox1* is expressed within CGE-derived but not MGE-derived cortical interneuron subtypes. GP, globus pallidus; HC, hippocampus; Str, striatum; Th, thalamus. Scale bars: **A–D, F**, 200 μ m; **E–J**, 50 μ m.

vious finding that *Prox1* transcription is induced by *Ascl1* (*Mash1*), a proneural factor expressed within all three ganglionic eminences (Torii et al., 1999). By E14.5, *Prox1* expression is increased in the subventricular zone of the CGE (Fig. 1C,D) and in addition, is observed within the cortex and is restricted primarily

to GABAergic interneuron populations, as indicated by *Dlx5/6* lineage fate mapping (Miyoshi et al., 2010; Fig. 1D'); *Prox1* is transiently expressed in Cajal–Retzius cells but shuts off by birth; data not shown). This timing coincides with the arrival of the earliest cohort of CGE-derived interneurons into the cortex (Mi-

yoshi et al., 2010), several days after MGE-derived interneurons begin to populate this structure (Anderson et al., 2001; Fogarty et al., 2007; Miyoshi et al., 2007; Xu et al., 2008). At E16.5, we observed that *Prox1*-positive GABAergic cells (Fig. 1E) coexpressed Sp8 (Fig. 1E'), a transcription factor selectively expressed in CGE-derived but not MGE-derived or POA-derived lineages (Ma et al., 2012). To further demonstrate that *Prox1* is selectively expressed within CGE-derived lineages, we generated a BAC transgenic *Cre* driver by using *cis*-regulatory elements of *Htr3A* gene (*Htr3ABAC-Cre*, GENSAT, also $\times 11.8$ enriched in CGE lineages; Table 1) and combined this with *Dlx5/6-Flpe* and a dual EGFP reporter (*RCE:dual*) to label CGE-derived interneuron precursors. We found that *Prox1* is expressed in the CGE-derived interneuron precursors labeled with the *Htr3ABAC-Cre* driver within the E16.5 cortex (data not shown). Consistent with these results, we did not observe *Prox1* expression in immature MGE-derived interneurons labeled with EGFP by using an inter-sectional genetic approach (Dymecki and Kim, 2007) that combined *Lhx6BAC-Cre* (Fogarty et al., 2007) and *Dlx5/6-Flpe* drivers with the *RCE:dual* reporter at E16.5 (Fig. 1F, F'). Interestingly, *Prox1* regulation within MGE-derived cells is lineage specific in that it entirely shuts off in cortical interneuron and globus pallidus populations (Fig. 1F; Flandin et al., 2010; Nóbrega-Pereira et al., 2010), but remains expressed in some striatal interneurons (Fig. 1F; Rubin and Kessaris, 2013).

We then analyzed the expression profile of *Prox1* in the P21 neocortex. Using immunohistochemistry, we observed that while a substantial number of cells were found to express *Prox1*, it was still completely excluded from MGE-derived interneurons (Fig. 1G–G'). To further analyze which specific subtypes of CGE-derived interneurons express *Prox1*, we took advantage of a conditional *Prox1* allele (*Prox1-C:EGFP*), which expresses EGFP under the control of the endogenous *Prox1* locus following Cre-mediated recombination (Iwano et al., 2012). We combined this line with a forebrain pan-GABAergic *Dlx6a-Cre* driver (Monory et al., 2006) to analyze the morphologies and molecular markers of *Prox1*-expressing cortical interneurons labeled with EGFP (*Dlx6a-Cre; Prox1-C:EGFP/+*). Within the P21 cortex, *Prox1* was detectable in most (84.3%) of the RELN-expressing (without SST) cells (Fig. 1H), although its expression levels in this population were somewhat variable (Fig. 1H, solid arrowheads). *Prox1* was also expressed in almost all (98.6%) of the VIP-positive cells (Fig. 1I, J) at P21 (Fig. 1K). Conversely, the large majority of *Prox1*-positive interneurons expressed either VIP or RELN, and only 7.7% were negative for both markers (Fig. 1K). These results are consistent with the previous finding that *Prox1* is expressed in CGE-derived interneuron subtypes (Rubin and Kessaris, 2013). We conclude that, while *Prox1* is uniformly expressed in the subventricular zones of the ganglionic eminences, within cortical interneuron lineages it is selectively maintained within CGE-derived subtypes into adulthood (Fig. 1K).

***Prox1* promotes the migration of CGE-derived interneuron precursors into superficial cortical layers**

To test the role of *Prox1* in CGE-derived interneurons, we used an additional conditional *Prox1* loss-of-function allele to generate *Prox1*-null cells at distinct developmental stages. In this conditional loss-of-function allele (*Prox1-F*), exons 2 and 3 that encode the homeodomain of *Prox1* are flanked by loxP sites (Harvey et al., 2005; Lavado et al., 2010), such that *Prox1* expression is ablated following Cre-mediated recombination. We combined this allele to the conditional *Prox1-C:EGFP* line (Fig. 1H–J), in which the entire coding region of *Prox1* is flanked by

loxP sites, such that recombination results in a null allele in addition to EGFP expression in *Prox1*-expressing cells. We combined both *Prox1* conditional alleles with a *Dlx6a-Cre* driver line (Monory et al., 2006), which allowed us to remove *Prox1* from the entire telencephalic GABAergic population as these cells transit through the subventricular zone. Using EGFP as a marker, we identified the *Prox1*-expressing population and compared the behavior of control (heterozygous: *Prox1-C:EGFP/+*) versus *Prox1* loss-of-function (null: *Prox1-C:EGFP/F*) cells (Fig. 2).

As we have previously shown, CGE-derived interneuron precursors are first observed migrating tangentially through the intermediate zone of the cortex at \sim E14.5 (Miyoshi et al., 2010). At this stage, both control and *Prox1* loss-of-function CGE-derived interneuron precursors exhibited comparable migration patterns within the cortex (Fig. 3A, B). This suggests that *Prox1* loss-of-function does not delay the initiation of tangential migration into the cortex. By E16.5, in the control cortex, we observed an increase in the number of cells in the cortical marginal zone and within the developing cortical plate (Fig. 2A), consistent with previous analyses (Miyoshi et al., 2010; Rubin et al., 2010). In contrast, fewer *Prox1*-null cells had migrated into the marginal zone and cortical plate, although the intermediate and subventricular zone populations were similar to controls (Fig. 2B, C). Two days later, at E18.5, in addition to the reduction of labeled cells located in the marginal zone and cortical plate, we observed an accumulation of *Prox1*-null cells in the intermediate and subventricular zones (Fig. 2D–F). This indicates that *Prox1* is required for the transition of CGE-derived interneuron precursors from the tangential migration stream into the cortical plate.

Next, we analyzed how the abnormal migration pattern we observed in *Prox1*-null cells during embryonic stages ultimately impacts their localization within the postnatal cortex. We compared the laminar distribution of EGFP(*Prox1*)-labeled control and *Prox1*-null cells at P7 (Fig. 2G, H), a stage at which most GABAergic interneurons have completed their migration within the cortex (Miyoshi and Fishell, 2011; Inamura et al., 2012). In the *Prox1* loss-of-function animals, we observed a marked reduction in EGFP-labeled cell numbers in layers I (47.9%) and II/III (64.5%) with a corresponding increase in layers V/VI (148.7%) compared with controls (Fig. 2I). This indicates that CGE-derived interneurons lacking *Prox1* function were displaced ectopically within deeper layers. Furthermore, while many EGFP-labeled control cells exhibited vertically oriented processes in the superficial layers (Fig. 2G), these morphologies were not similarly evident in *Prox1* loss-of-function cells (Fig. 2H).

Loss of *Prox1* results in dysregulation of relatively few genes within CGE-derived interneuron precursors

We next examined whether *Prox1* was required for the expression of the candidate CGE transcription factors *CoupTFII* (Tripathi et al., 2004; Kanatani et al., 2008; Miyoshi et al., 2010; Cai et al., 2013) and *Sp8* (Waclaw et al., 2006; Ma et al., 2012) but found no differences between control and loss-of-function cortices (Fig. 3C–F). Thus to uncover the molecular mechanisms underlying the impaired transition of *Prox1* loss-of-function cells from the intermediate to marginal zone, we performed an unbiased microarray expression analysis comparing EGFP-labeled control versus *Prox1* loss-of-function interneurons that were FACS purified from the E18.5 cortex. Somewhat surprisingly, we observed significant changes in only a small number of genes (79 genes including 46 upregulated and 33 downregulated genes, fold

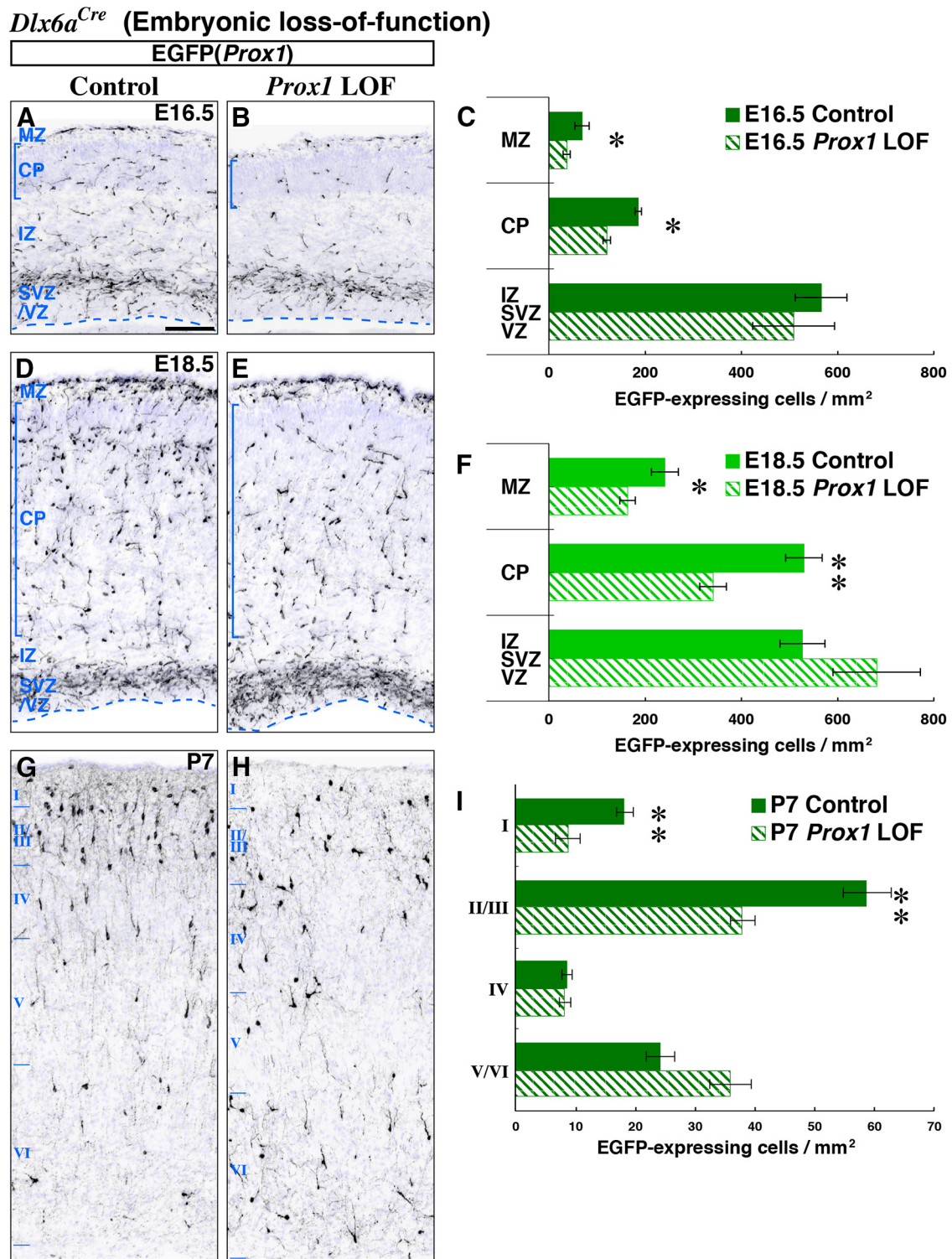


Figure 2. *Prox1* promotes the superficial layer positioning of CGE-derived interneurons by regulating embryonic tangential migration. Localization of EGFP(*Prox1*)-labeled control (*Dlx6a-Cre; Prox1-C:EGFP/+*) and *Prox1* loss-of-function (*Dlx6a-Cre; Prox1-C:EGFP/F*) GABAergic cells were analyzed within the cortex (shown in black). Nuclear counter staining by DAPI is shown in blue. **A, B**, While we found no delay in the initiation of tangential migration from the CGE into the cortex of *Prox1* loss-of-function at E14.5 (Fig. 3 *A, B*), by E16.5, we observed a decrease in *Prox1*-null EGFP-labeled cells reaching the marginal zone (MZ) and cortical plate (CP). Comparable numbers of EGFP-labeled cells are found in the intermediate and subventricular/ventricular zones (IZ and SVZ/VZ). **C**, Bar graphs comparing the cortical area normalized distribution of EGFP-labeled (GABAergic *Prox1*) cells at E16.5 in the control (filled) and *Prox1* loss-of-function (LOF, shaded) experiments. Two-tailed *t* test: $p = 0.0255^*$ (MZ), $p = 0.0172^*$ (CP), $p = 0.425$ (IZ/SVZ/VZ). **D–F**, By E18.5, in addition to the loss in marginal zone and cortical plate, more EGFP-labeled cells were observed within the intermediate zone and SVZ/VZ of the conditional *Prox1* loss-of-function cortices. For the sake of clarity, hippocampal areas are cropped from the figures (bottom). Two-tailed *t* test: $p = 0.0156^*$ (MZ), $p = 0.00893^{***}$ (CP), $p = 0.132$ (IZ/SVZ/VZ). **G–I**, At P7, mutant cells were decreased in superficial (I–III) layers, but increased in deep (V, VI) layers compared with the control cortex. Two-tailed *t* test: $p = 0.00693^{**}$ (I), $p = 0.00960^{**}$ (II/III), $p = 0.837$ (IV), $p = 0.0842$ (V/VI). In addition, the population of cells with vertically oriented processes that is normally found in the superficial layers (**G**) was less obvious in the *Prox1* loss-of-function cortex (**H**). All error bars indicate SEM. Scale bar, 50 μ m.

change > 1.5 , p value < 0.05 ; data not shown), including downregulation of *Vip* ($\times 14.15$), *Cck* ($\times 3.22$), and *Calb2* (Calretinin, $\times 1.79$), markers that are expressed within mature CGE-derived interneuron subtypes (Table 3).

Previous work has shown that *Dlx1/2* activity induces the expression of the transcription factor *Arx* (Cobos et al., 2005a; Colasante et al., 2008), promoting migration by suppressing neurite growth mediated by Pak3, a p21-activated serine/threonine kinase that acts as a downstream effector of the Rho family of GTPases (Cobos et al., 2007). However, in our microarray analysis comparing gene expression levels in control versus *Prox1* loss-of-function cells, we did not reveal any measurable change in *Pak3*, *Arx*, or any of the *Dlx*-gene family members (data not shown). These data strongly suggest that the migration of CGE-derived interneuron precursors is independently regulated by the *Dlx1/2* and *Prox1* transcription factors.

Subtype-specific requirement for *Prox1* in the differentiation of CGE-derived cortical interneurons

To further characterize the later effects of *Prox1* loss-of-function on CGE-derived interneuron subtypes following their differentiation, we analyzed control and conditional (*Dlx6a-Cre*) *Prox1* loss-of-function cells at P21, when interneurons have acquired their characteristic molecular markers and intrinsic electrophysiological properties. Consistent with what we have observed at P7, we found that the abnormalities in the layer distribution of EGFP-labeled cells persisted at P21, with a decrease in layers I–IV and increase in layer VI in the mutant (Fig. 4I). The total number of EGFP-expressing *Prox1* cells in mutants compared with controls was reduced at P7 (82.8% of control numbers) and further decreased by P21 (74.6% of control numbers; Fig. 4J), suggesting that *Prox1* is important for the maintenance of CGE-derived cortical interneurons even after they have reached their final laminar locations. Because the *Dlx6a-Cre* driver removes *Prox1* broadly throughout the ventral telencephalic subventricular zones, we tested the specific requirement for *Prox1* in CGE-derived interneurons. To do so, we used an *Htr3ABAC-Cre* driver to remove *Prox1* only in the migrating postmitotic interneuron precursors derived from the CGE (Fig. 5). By combining with a Cre-dependent tdTomato (*Ai9: R26R-CAG-loxPstop-tdTomato-WPRE polyA*; Madisen et al., 2010) and *Prox1-C:EGFP* conditional reporter lines, we observed that the *Htr3ABAC-Cre* driver targets a subpopulation of

Dlx6a^{Cre} (Embryonic loss-of-function)

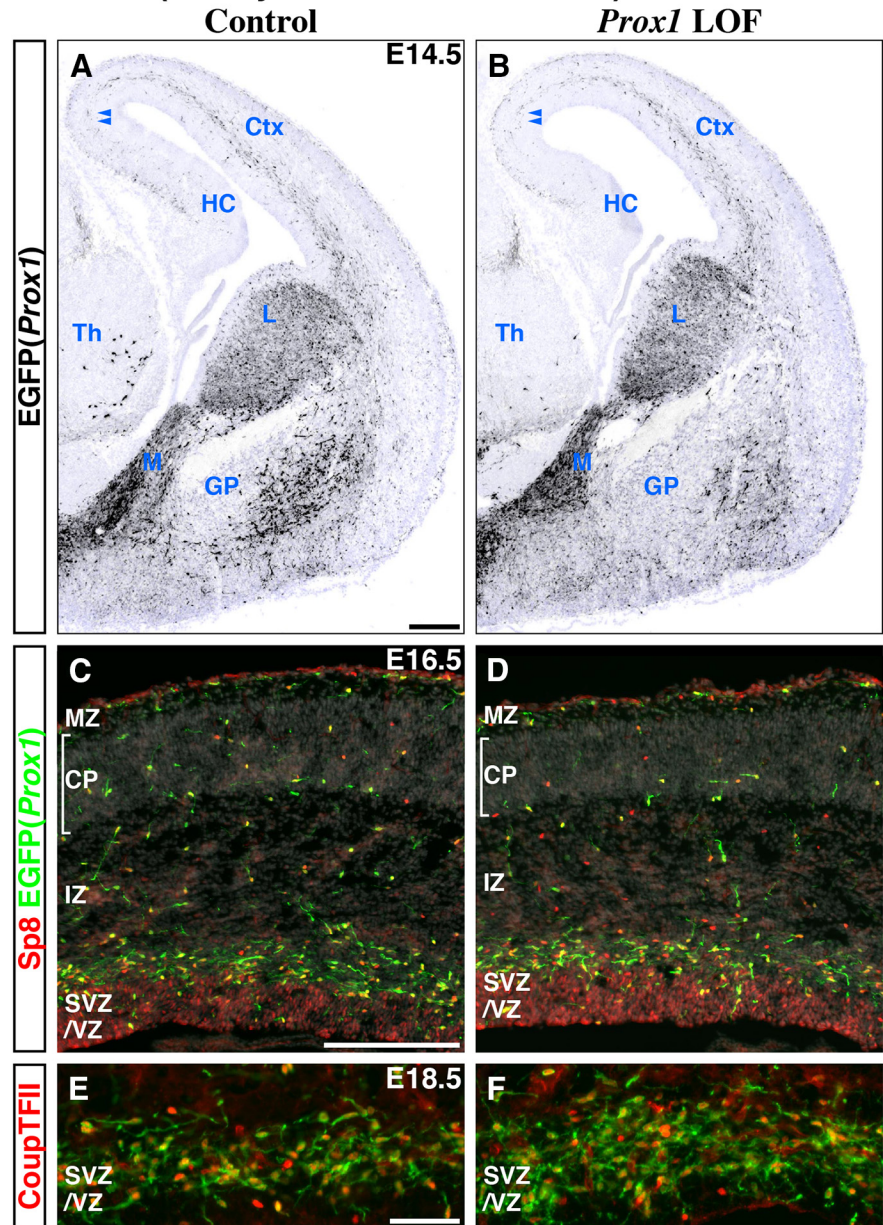


Figure 3. Embryonic (*Dlx6a-Cre*) *Prox1* loss-of-function does not affect the interneuron precursors for their tangential migration from the CGE into the developing cortex as well as the expression of Sp8 and CoupTFII transcription factors. We performed embryonic (*Dlx6a-Cre*) control (**A, C, E**) and *Prox1* loss-of-function (*Prox1-C:EGFP/+* and **F**) experiments (**B, D, F**). **A, B**, At E14.5, about the time the earliest cohort of CGE-derived interneuron precursors is first observed tangentially migrating through the intermediate zone (IZ) of the cortex (Miyoshi et al., 2010), we found no obvious differences between control and *Prox1*-null cells labeled with EGFP (shown in black) with regard to their migration pattern or distance from the CGE. Nuclear counter staining by DAPI is shown in blue. Double arrowheads indicate the CGE-derived interneuron precursors that have reached the border area between the hippocampus (HC) and cortex (Ctx). While control EGFP(*Prox1*)-labeled cells are positioned laterally to the developing globus pallidus (GP) and do not express CoupTFII (*Nr2f2*), in the *Prox1* loss-of-function ventral telencephalon, very few EGFP(*Prox1*)-labeled cells are observed in the comparable domain. **C, D**, In addition to its expression within cortical progenitors, at E16.5, the Sp8 expression pattern within EGFP(*Prox1*)-labeled cells is comparable between the control and *Prox1* loss-of-function cortex. **E, F**, Higher magnification pictures of the cortical subventricular/ventricular zones (SVZ/NZ) in Figure 2D and E. While there are significantly more EGFP-labeled cells found in the SVZ/NZ of the *Prox1* loss-of-function cortex at E18.5 (see also Fig. 2F), the proportion of CoupTFII expression within EGFP(*Prox1*)-labeled cells is not changed. M, MGE; L, LGE; Th, thalamus; MZ, marginal zone; CP, cortical plate. Scale bars: **A–D**, 200 μ m; **E, F**, 50 μ m.

migrating CGE-derived interneurons expressing *Prox1* (Fig. 5A–C; data not shown). Even though this *Htr3ABAC-Cre* driver exhibited less efficient recombination compared with the *Dlx6a-Cre* driver (Figs., 2A, D, 3A) resulting in a milder

Dlx6a^{Cre} (Embryonic loss-of-function)

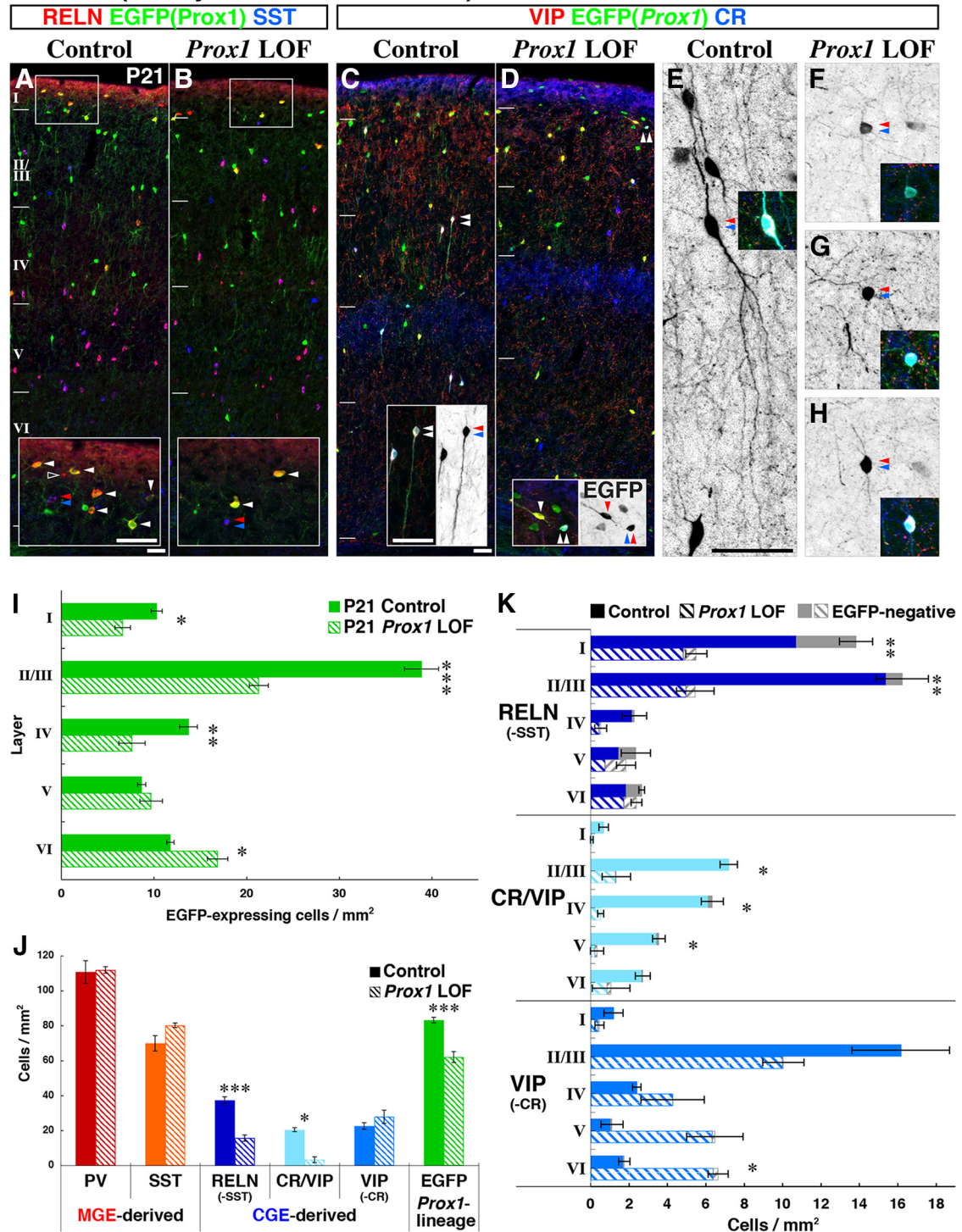


Figure 4. Subtype-specific requirement for *Prox1* in CGE-derived GABAergic cortical interneuron development. **A, B**, Immunohistochemistry for RELN/SST on EGFP(*Prox1*)-labeled cells in control and *Prox1* loss-of-function (*Dlx6a-Cre; Prox1-C:EGFP*^{+/+} and */-*) cortices at P21. While RELN-expressing cells (negative for SST) expressed EGFP at variable levels (arrowheads), they were generally reduced in the superficial layers of conditional *Prox1* loss-of-function cortices (**B**). Open arrowhead indicates the EGFP(*Prox1*)-negative RELN cells and double arrowheads indicate MGE-derived SST/RELN-expressing interneurons. **C, D**, Characterization of CR, VIP, and EGFP-positive cell profiles at P21. Double and single arrowheads indicate CR/VIP or VIP-single interneurons, respectively. While CR/VIP cells were severely reduced in mutants, the total numbers of VIP-single cells was unchanged. Furthermore, the remaining CR/VIP cells in mutants (**D**, double arrowheads) did not exhibit the characteristic bipolar morphology observed in controls (**C**). **E–H**, To better visualize the morphologies in *Prox1*-null CR/VIP interneurons, stacked views from confocal microscopy images were generated. CR/VIP-expressing cells (double arrowhead and inset) are found with bipolar morphology (**E**). In contrast, none of the CR/VIP-expressing cells remaining in the *Prox1* loss-of-function cortex exhibit typical bipolar morphology (**F–H**). The best example of a mutant cell that we found to retain bipolar morphology to some extent is shown in **H**, but in most cases, obvious processes protruding from the soma could not be found (**F, G**). **I**, Layer distribution of EGFP(*Prox1*)-labeled control (filled bars) and *Prox1* loss-of-function (LOF) cells (shaded bars) at P21. At P21, EGFP-labeled *Prox1*-null cells were displaced within deeper layers of the cortex, similar to the phenotype observed at P7 (Fig. 2I). Two-tailed *t* test: $p = 0.0133^*(I)$, $p = 0.000380^{***}(II/III)$, $p = 0.00376^{**}(IV)$, $p = 0.463(V)$, $p = 0.0148^*(VI)$. **J**, Molecular expression profiles of interneurons in the P21 somatosensory barrel cortex for control and *Prox1* loss-of-function experiments. The total numbers of PV(Pvalb)-expressing (red) and SST-expressing (orange) interneurons were not altered in the mutant. RELN (SST-negative) cell numbers were reduced to (Figure legend continues.)

phenotype, we still observed a similar displacement of EGFP-labeled cells into the deeper cortical layers (Fig. 5D–H).

We next compared the molecular expression profiles of interneurons within the P21 cortices of control and *Prox1* conditional loss-of-function animals (Fig. 4A–D). Within the P21 cortex, we did not observe any obvious changes in the distribution and numbers of PV-expressing and SST-expressing cells (Fig. 4A,B, red and orange bar graphs in J), indicating that *Prox1* expression within the MGE subventricular zone is not required for the development of MGE-derived cortical interneurons.

CGE-derived interneurons can be divided into three broad classes based on their molecular expression profiles (Fig. 1K; Miyoshi et al., 2010) of RELN (SST negative), CR/VIP double, and VIP single (CR negative). In the cortices of conditional *Prox1* loss-of-function animals, the total number of RELN-expressing (without SST) cells, a population that is largely comprised by neurogliaform and dense plexus morphologies (Miyoshi et al., 2010; Fig. 4A,B), was reduced to 42% of control numbers (Fig. 4J, dark blue bars). The loss of RELN-expressing (SST-negative) cells was particularly prominent in layers I–IV (Fig. 4K, top). Interestingly, loss of RELN-expressing cells was also observed in the *Prox1*-negative population (Fig. 4K, gray bars). This suggests the ~15% of the RELN-positive population that does not express *Prox1* in the P21 cortex (Figs. 1H, 4A, open arrowhead) likely still required this gene earlier during development.

We next examined the remaining two broad classes of CGE-derived interneurons, CR/VIP coexpressing and VIP-single (CR-negative) populations, both of which exhibit primarily bipolar/bifurcated morphologies (Fig. 4C–H). Strikingly, the CR/VIP double-positive population was severely reduced across all cortical layers in the mutants (Fig. 4K, middle) to 16% of control numbers (Fig. 4J). Furthermore, the very few CR/VIP double-positive cells that remained lacked their characteristic bipolar morphology (Fig. 4C,D, insets; E–H, confocal stack images). Late embryonic removal of *Prox1* with the CGE-specific driver *Htr3ABAC-Cre* also resulted in a decrease in CR/VIP cells (Fig. 5I), although the effect was less pronounced than that observed with the early embryonic *Dlx6a-Cre* driver, consistent with the milder layer displacement of *Htr3ABAC-Cre Prox1*-null cells (Fig. 5H). In addition, not all of the CR/VIP-expressing *Prox1*-null cells lost the bipolar morphologies in this late embryonic removal (Fig. 5G,G'). Regarding the VIP-single cells, although we did not observe any obvious change in the total number of cells (Fig. 4J), following the general trend of deep layer displacement observed in the *Prox1* loss-of-function population (Fig. 4I), they were decreased in the superficial (I–III) and correspondingly increased in the deep (IV–VI) cortical layers (Fig. 4K, bottom).

←

(Figure legend continued.) ~40%, CR/VIP-interneurons were severely reduced, and the VIP-single population was unaltered. Overall, EGFP(*Prox1*)-expressing cells were reduced to 75% in the *Prox1* loss-of-function mutant at P21. Two-tailed *t* test: $p = 0.880$ (PV), $p = 0.0905$ (SST), $p = 0.000334$ ***(RELN), $p = 0.0236$ *(CR/VIP), $p = 0.403$ (VIP), $p = 0.00169$ ***(EGFP). K, The laminar distribution of each RELN, CR/VIP, and VIP-single interneuron subtype is shown. In addition to control (filled bars) and *Prox1* loss-of-function (shaded bars), gray bars indicate the EGFP-negative population of each subtype. While the RELN-positive population was primarily reduced in the superficial (I–IV) layers, CR/VIP-expressing cells were reduced in all layers. The VIP-single population was reduced in superficial (I–III) and increased in deep (IV–VI) layers and thus was ectopically displaced into deeper layers. Statistics are shown for the marker-positive profiles including both EGFP-positive and EGFP-negative cells. Two-tailed *t* test: $p = 0.00437$ ***, $p = 0.00127$ ***, $p = 0.1841$, $p = 0.6411$, $p = 0.551$ (I–VI, RELN), $p = 0.188$, $p = 0.0369$ *, $p = 0.0136$ *, $p = 0.0371$ *, $p = 0.316$ (I–VI, CR/VIP), $p = 0.216$, $p = 0.148$, $p = 0.414$, $p = 0.0507$, $p = 0.0164$ * (I–VI, VIP). All error bars are SEM. Scale bars, 50 μ m.

To further characterize the requirement of *Prox1* in the differentiation of CGE-derived interneurons, we performed whole-cell patch-clamp recordings from EGFP-positive cells in acute brain slices (P16–P20) and analyzed their intrinsic electrophysiological properties. While we excluded the residual CR/VIP interneurons from our analysis due to severity of the null phenotype in these cells (Fig. 4F–H), all of the *Prox1* loss-of-function cells we recorded in the superficial layers (I–III; 24 cells) exhibited normal resting membrane potential, displayed overshooting action potentials (APs), and could sustain high-frequency AP discharge (data not shown). Based on their membrane properties and discharge characteristics, we were able to assign the recorded cells to the previously reported CGE-derived subtype categories (Butt et al., 2005; Miyoshi et al., 2010), suggesting that their electrophysiological differentiation is largely unaffected by *Prox1* loss of function. From the *Prox1* loss-of-function cells recorded in layer I (17 cells), all of which were *post hoc* identified as RELN positive and VIP negative (Fig. 6A,B, middle), we found five late-spiking (LS; Fig. 6B), five initial-adapting, five type 1 bursting non-adapting, and one delayed intrinsic-bursting interneuron, and one cell that could not be classified. Analysis of LS neurogliaform cells (Chu et al., 2003; Tamas et al., 2003; Kubota et al., 2011; DeFelipe et al., 2013; Ma et al., 2014; Pohlkamp et al., 2014) that are one of the most characteristic subtypes residing in layer I and expressing RELN did not reveal any differences across a variety of intrinsic electrophysiological measures when comparing control and *Prox1*-null cells (Fig. 6A,B). From the seven EGFP-positive *Prox1* loss-of-function cells recorded in layers II/III, six were *post hoc* identified as VIP positive and negative for CR (Fig. 6D,E, middle). In these cells, we found three irregular-spiking (IS) and two type 3 delayed non-fast spiking (dNFS3) interneurons and one cell that could not be classified (Miyoshi et al., 2010). Similar to the RELN-positive classes, VIP-expressing dNFS3 (Fig. 6E) and IS (data not shown) subtypes appeared to have normal passive and active membrane properties (Fig. 6D).

We next analyzed the sEPSCs received by control and *Prox1*-null cells as a measure of their network integration. All cells recorded received sEPSCs, but remarkably, VIP-positive *Prox1* loss-of-function cells in layers II/III showed a marked reduction in the number but not the amplitude of these events (Fig. 6D,E, bottom, F). Since *Prox1*-null VIP-single cells that were not displaced but were properly located in layers II/III still showed a significant reduction in the sEPSCs they receive (Fig. 6F), this interneuron subtype appears to require *Prox1* function to properly integrate into the cortical network. In contrast, the *Prox1* loss-of-function LS cells received a comparable number of excitatory events with similar amplitude to the control cells (Fig. 6A,B, bottom, C). Thus we found a selective decrease in the excitatory drive onto VIP-single but not RELN-expressing populations after the removal of *Prox1*.

Our early embryonic (*Dlx6a-Cre*) loss-of-function experiments on forebrain GABAergic interneuron populations demonstrate a subtype-specific requirement for *Prox1* within all CGE-derived interneurons. RELN-expressing cells were reduced from the superficial layers by ~40%, and CR/VIP double-positive cells were largely eliminated from the cortex. Moreover, the CR/VIP cells that persisted failed to acquire their characteristic bipolar morphology. Finally, the VIP-single population was displaced into deeper layers, and even properly located cells exhibited a severe reduction in excitatory input.

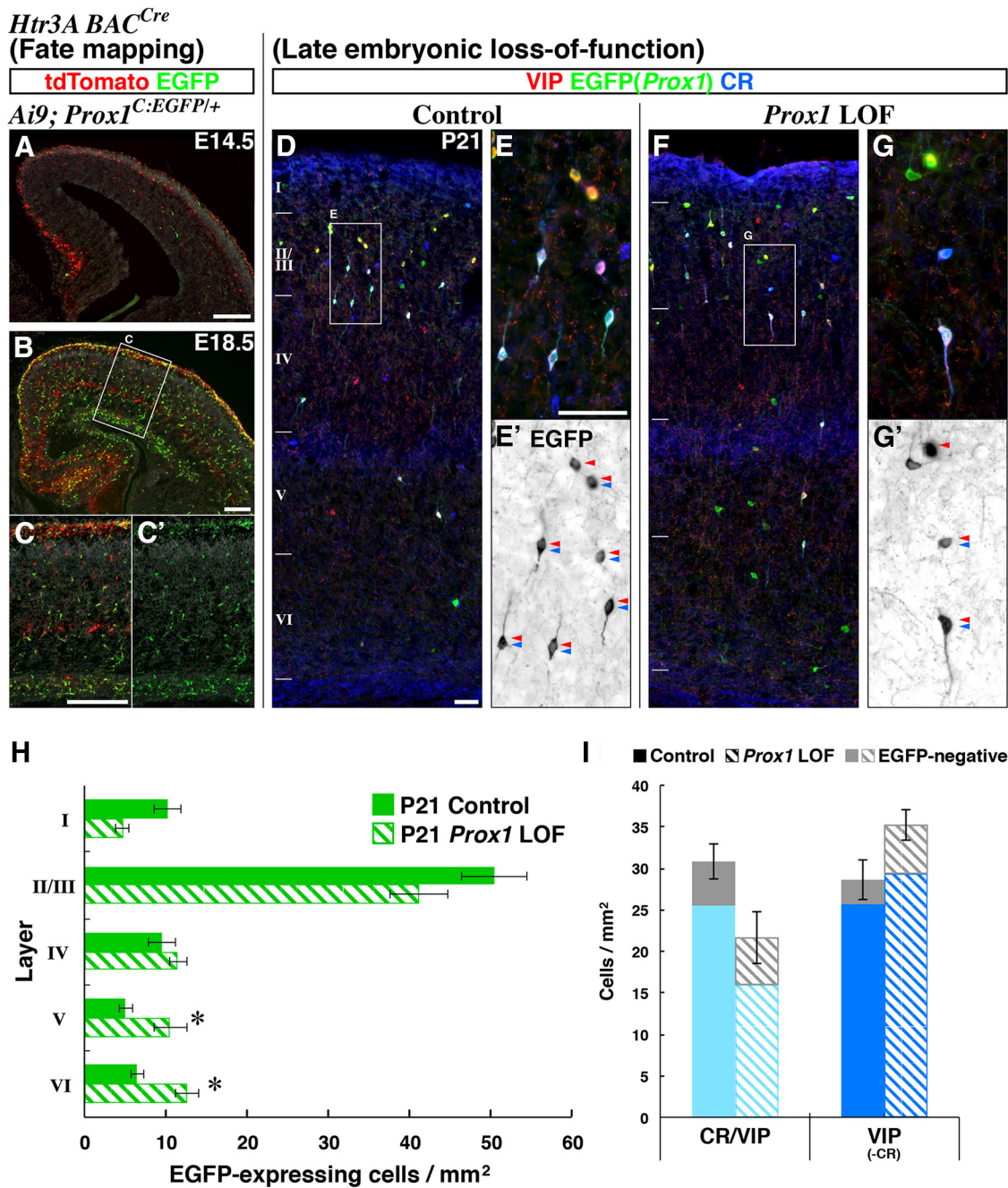


Figure 5. Late embryonic (*Htr3ABAC-Cre*) *Prox1* loss-of-function (LOF) in CGE-derived interneurons shows similar but milder phenotypes compared with pan-GABAergic early embryonic (*Dlx6a-Cre*) removal. We used the *Htr3ABAC-Cre* driver to restrict recombination to CGE-derived lineages. This driver recombines the *Prox1-C:EGFP* allele at somewhat later stages of embryonic cell migration than *Dlx6a-Cre* (Figs. 2–4) in a subpopulation of CGE-derived cells. **A–C**, Recombination efficiency of the *Htr3ABAC-Cre* driver was addressed by analyzing crosses with *Prox1-C:EGFP/+* and *Ai9* reporter (*R26R-CAG-loxPstop-tdTomato-WPRE polyA*) lines in the same animal at E14.5 (**A**) and E18.5 (**B**, **C**). At E14.5, the *Htr3ABAC-Cre* driver (**A**) resulted in fewer EGFP-expressing cells within the cortex compared with the *Dlx6a-Cre* driver (Fig. 3A). At E18.5, substantial numbers of EGFP-labeled cells were evident in the cortex, although to a lesser extent when compared with the *Dlx6a-Cre* driver (Fig. 2D). **C**, **C'**, A higher magnification view of **B** also shown for EGFP signals only (**C'**). The *Htr3ABAC-Cre* driver also targets non-GABAergic populations, most likely the Cajal–Retzius and subplate cells (red without green), in addition to CGE-derived interneuron precursors. **D–G**, Comparison of control and *Prox1* loss-of-function (*Htr3ABAC-Cre; Prox1-C:EGFP/+* and **F**) cells at P21. **E**, **G**, Higher magnification of the areas in **D** and **F** are presented and EGFP signals are shown in black (**E'**, **G'**). Double arrowheads indicate CR/VIP-expressing cells and single arrowheads indicate VIP-single (CR-negative) cells. In contrast to what we observed in the early embryonic (*Dlx6a-Cre*) *Prox1* loss-of-function study, in the *Htr3ABAC-Cre* mutant, not all of the remaining CR/VIP cells lost their characteristic bipolar morphologies (**G'**). While the CR/VIP *Prox1*-null cell in the middle has a round morphology with no obvious processes, the cell at the bottom exhibits a bipolar morphology (**G'**). **H**, A graph indicating the layering of late embryonic (*Htr3ABAC-Cre*) *Prox1* loss-of-function cells in P21 cortex. Note that the decrease (Layers I–III) and increase (Layers V/VI) found in the EGFP-expressing cells of *Prox1* loss-of-function cortex are consistent but milder compared with the results observed from the early embryonic (*Dlx6a-Cre*) loss-of-function (Fig. 4). Two-tailed *t* test: $p = 0.0636$ (I), $p = 0.212$ (II/III), $p = 0.359$ (IV), $p = 0.0412^*$ (V), $p = 0.0205^*$ (VI). **I**, Cell numbers of CR/VIP-expressing and VIP-single populations in the P21 cortex of control and late embryonic *Prox1* loss-of-function animals (shaded bars). EGFP(*Prox1*)-negative populations are shown in gray bars. Consistent with the early embryonic (*Dlx6a-Cre*) loss-of-function, we also observed a reduction in CR/VIP-expressing cells, with no obvious change in the VIP-single population following late embryonic (*Htr3ABAC-Cre*) loss-of-function. Note that the recombination mediated by the *Htr3ABAC-Cre* driver does not take place in all CGE-derived population at P21 in either control or *Prox1* loss-of-function animals (gray bars) compared with that observed when the *Dlx6a-Cre* driver was used (Figs. 1I–K, 4K). Two-tailed *t* test: $p = 0.0852$ (CR/VIP), $p = 0.0786$ (VIP). Error bars indicate SEM. Scale bars: **A–C**, 200 μ m; **D–G**, 50 μ m.

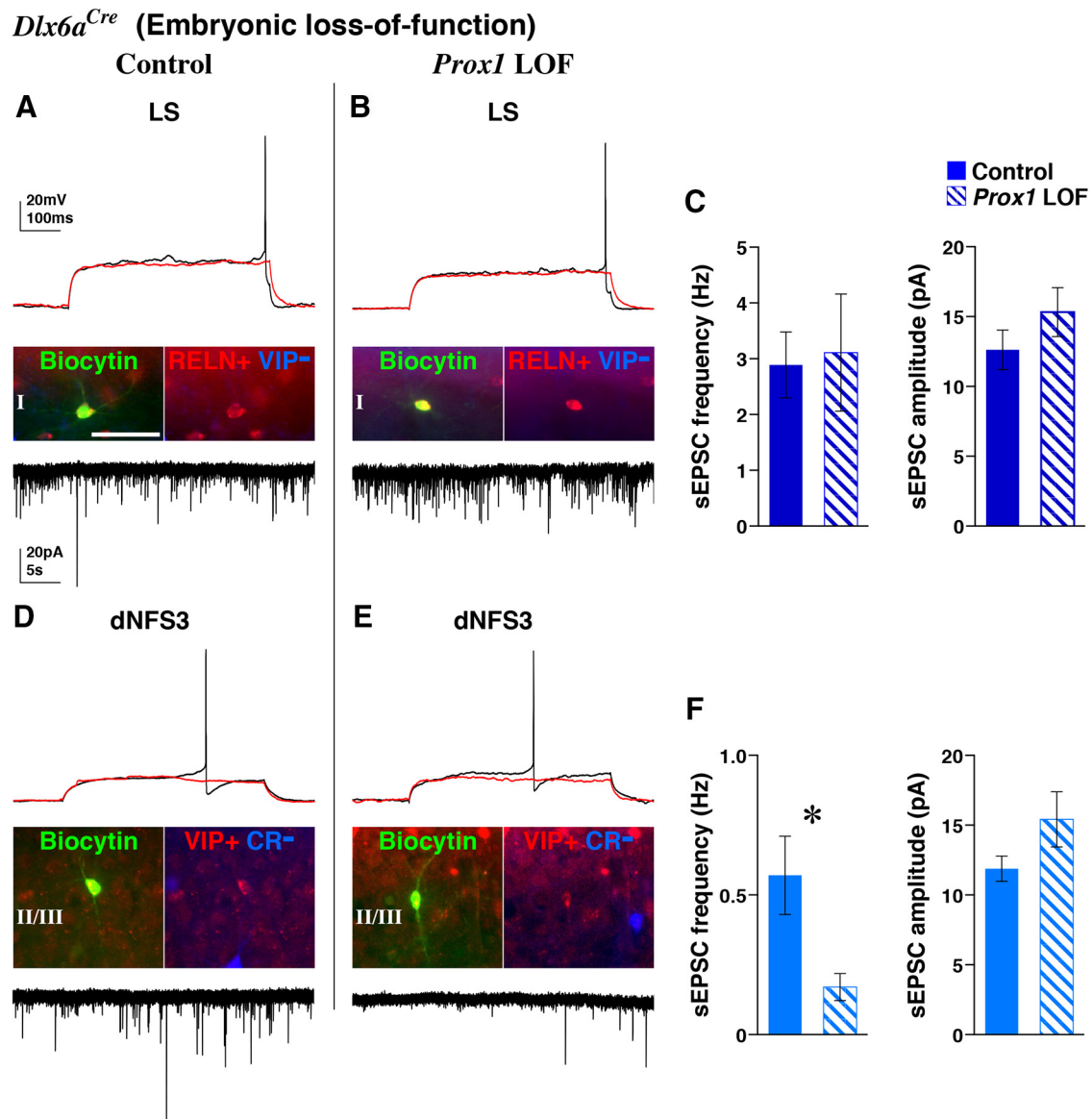


Figure 6. Reduction of excitatory events in VIP-single cortical interneurons following embryonic (*Dlx6a-Cre*) *Prox1* removal. Control and embryonic (*Dlx6a-Cre*) *Prox1* loss-of-function (LOF) cells labeled with EGFP were recorded in brain slices of the somatosensory cortex (P16–P20). Subsequent to electrophysiological analysis and biocytin filling, *post hoc* immunohistochemistry for RELN/VIP or CR/VIP was performed. **A**, A control cell that was identified by *post hoc* analysis to be positive for RELN but not VIP showed characteristic LS firing at near threshold (top, black trace; red trace is at subthreshold) and received sEPSCs at a frequency of 3 Hz (bottom trace). **B**, A *Prox1*-null RELN-positive VIP-negative cell showed a similar LS action potential discharge and received sEPSCs at a comparable frequency and amplitude to that of control cells (**A**). **C**, Analysis of the frequency (left) and amplitude (right) of sEPSCs in the control ($n = 6$) and *Prox1* loss-of-function LS cells ($n = 4$, shaded bars) shows that these interneurons do not require *Prox1* for the establishment of proper excitatory inputs. Mann–Whitney: $p = 0.187$ (frequency), $p = 0.442$ (amplitude). **D**, A representative example of a VIP-single (CR-negative) control cell with dNFS3 firing properties, with the sEPSCs it receives shown at the bottom. **E**, A trace of a dNFS3 cell (VIP-positive CR-negative) lacking *Prox1*. **F**, In contrast to RELN-positive LS cells (**C**), *Prox1*-null VIP-single interneurons ($n = 4$) show a dramatic reduction in the frequency of sEPSCs (left) compared with control cells ($n = 4$). Nevertheless, the amplitude of sEPSCs shows no change (right). Mann–Whitney: $p = 0.0397^*$ (frequency), $p = 0.191$ (amplitude). Scale bar, 50 μm .

Prox1 has a postnatal role in the maturation of CGE-derived interneurons

To distinguish between early and late roles for *Prox1* in the development of CGE-derived interneurons (Fig. 1), we sought to examine the consequences of removing this gene during the postnatal maturation period after CGE-derived interneurons have already settled into their final laminar positions. To achieve this, we focused on the VIP-positive population, which broadly expresses *Prox1* (Fig. 1I–K) and also includes the most severely affected population, the CR/VIP coexpressing subtype.

We first analyzed the timing of *Prox1* removal with the *Vip-Cre* driver line (Taniguchi et al., 2011) by combining with a Cre-dependent tdTomato reporter line (*Ai9*) in control (*Prox1-C:*

EGFP/+) and *Prox1* loss-of-function (*Prox1-C:EGFP/F*) experiments. While at \sim E18.5 we found very few cells labeled for EGFP and tdTomato in the developing cortex (data not shown), later by P7, we observed efficient and overlapping recombination in the *Prox1-C:EGFP* allele and tdTomato reporter in both control (Fig. 7A) and loss-of-function (Fig. 7B) cortices. Thus the *Vip-Cre* driver line appeared to be well suited for us to perform postnatal *Prox1* loss-of-function experiments. At P7, we observed comparable cell numbers and layer distributions of control and *Prox1*-null interneurons (Fig. 7H, top; total recombined cells in the *Prox1* mutant was 97.4% of that in controls). This finding supports the idea that the layer displacement of VIP-single interneurons in the embryonic (*Dlx6a-Cre*) *Prox1* loss-of-function cortex (Figs. 2I, 4I,K) results

Vip^{Cre/+}; *Ai9* (Postnatal loss-of-function)

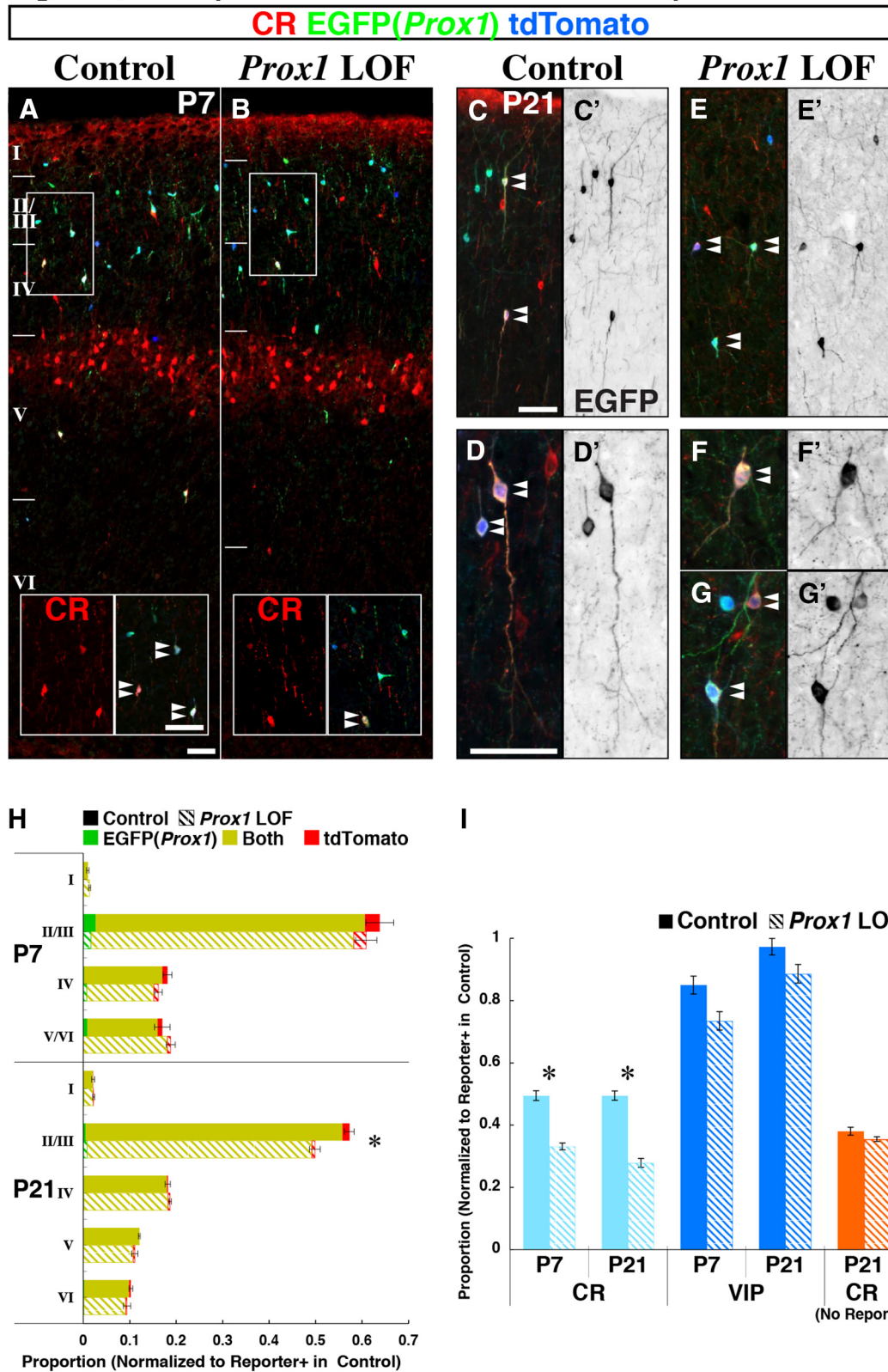


Figure 7. Postnatally (*Vip-Cre*), *Prox1* is required for the differentiation and survival of CR/VIP interneurons. Postnatal conditional loss-of-function (LOF) of *Prox1* was performed specifically within VIP-expressing interneurons with the *Vip-Cre* driver. *Vip*-positive cells were labeled independently of *Prox1* expression by combining the tdTomato reporter (*Ai9*) with the control or *Prox1* loss-of-function (*Prox1-C:EGFP/+* or */F*) alleles. This *Vip-Cre* driver initiates recombination in the *Prox1-C:EGFP* allele only after E18.5 (data not shown), thus allowing us to perform postnatal loss-of-function studies. **A, B**, By P7, we observed efficient recombination in both the tdTomato reporter and conditional *Prox1-C:EGFP* alleles in control and mutant cortices. In controls, VIP-positive interneurons exhibited a mature profile of CR (Calb2) expression by P7 (**A**, inset, double arrowheads), whereas in mutants, fewer cells expressed CR (**B**, inset). Note that layer Va pyramidal neurons have not downregulated CR at P7. **C–G**, Still, by P21, mutants exhibited a reduction in CR expression compared with controls, and those that remained did not show (*Figure legend continues*.)

from the failure of cells to transit from the intermediate zone into the cortical plate, rather than from impaired radial migration inside the cortical plate that occurs subsequently during the first postnatal week (Miyoshi and Fishell, 2011). However, by P21 (Fig. 7C–G), in the *Prox1* loss-of-function mutant we observed a progressive decrease in the number of labeled cells specifically in layers II/III (Fig. 7H, bottom). This indicates that sustained *Prox1* expression enhances the survival of *Vip-Cre*-labeled interneurons during the postnatal period between P7 and P21.

Although at P7 the layer distribution of *Vip-Cre*-labeled cells was not different between the control and conditional *Prox1* loss-of-function cells (Fig. 7H), we did observe changes in their molecular expression profiles. While approximately half (49.4%) of the *Vip-Cre*-labeled control population expressed CR at P7, there was a 30% decrease in CR expression in the mutant (33.2 vs 49.4% of total reporter-labeled population in control; Fig. 7I). Consistent with the cell loss found between P7 and P21, we observed a further reduction in CR expression in the mutant at P21 (Fig. 7I; control: 49.5% and mutant: 27.9% of total labeled cells in control). Furthermore, at this age, we observed morphological defects in the CR-expressing mutant cells that persisted in the adult cortex (Fig. 7E–G, double arrowheads, E'–G'). Although not as severely affected as the cells in the embryonic (*Dlx6a-Cre*) and late-embryonic (*Htr3ABAC-Cre*) *Prox1* loss-of-function brains (Figs. 4F–H, 5G), CR/VIP-expressing cells in the *Vip-Cre* mutant still exhibited some defects in acquiring their characteristic bipolar morphologies (Fig. 7E–G, E'–G', double arrowheads). We also analyzed the CR-expressing cells that were not labeled by *Vip-Cre*, the majority of which are derived from the MGE and coexpress SST (Fig. 1K), and as expected, they were unaffected in mutant animals at P21 (Fig. 7I, orange bars). Regarding the expression of VIP itself as detected by immunohistochemistry, at P7, we did observe a slight delay in the onset of its expression in conditional loss-of-function animals, but this recovered by P21 (Fig. 7I; reduction in VIP matches the cell loss at P21 shown in Fig. 7H, bottom).

From our postnatal (*Vip-Cre*) loss-of-function analysis, we conclude that *Prox1* is necessary in the CR/VIP subclass for the proper morphogenesis, CR expression, and survival of cells after the age of P7.

←

(Figure legend continued.) the similar characteristic bipolar morphologies observed in controls (C, D), but had kinked processes (E–G, double arrowheads). To better visualize cell morphology, EGFP is shown in black to the right of C–G (C'–G'). H, The laminar distribution of control and postnatal (*Vip-Cre*) *Prox1* loss-of-function cells in the cortex at P7 and P21. While there was no obvious difference between the control and postnatal *Prox1* conditional mutant at P7, by P21, cells were specifically reduced in layers II/III of the mutant. EGFP(*Prox1*) labeling and tdTomato expression (*Ai9* reporter) are shown in green and red, respectively, and the overlap is indicated by yellow. Two-tailed *t* test: $p = 0.127$, $p = 0.620$, $p = 0.577$, $p = 0.756$ (I–V/VI, P7), $p = 0.953$, $p = 0.0301^*$, $p = 0.735$, $p = 0.467$, $p = 0.648$ (I–VI, P21), $p = 0.700$, $p = 0.121$ (total numbers for P7 and P21). Error bars indicate SEM for total number of recombined cells in each layer. I, CR and VIP expressions were analyzed in postnatal (*Vip-Cre*) *Prox1* conditional mutants (labeled green and/or red) at P7 and P21. Values are shown as the proportion of labeled cells normalized to the total number of control cells at each age. While there was no change in the reporter-positive cell numbers at P7 (H), CR expression was decreased in the mutant compared with control at both ages. VIP expression was delayed in onset (P7) but recovered by P21 (the loss of VIP at P21 matches the cell loss in H, bottom). Reporter-negative CR-expressing cells (orange), most of which are derived from the MGE and coexpress SST, showed no change at P21. Two-tailed *t* test: $p = 0.0143^*$ (CR P7), $p = 0.0120^*$ (CR P21), $p = 0.383$ (VIP P7), $p = 0.198$ (VIP P21), $p = 0.562$ (CR, no reporter). Error bars represent SEM. Scale bars: 50 μ m.

***Prox1* cell-autonomously specifies the CR/VIP subtype of CGE-derived interneurons independent of its role in tangential migration**

Although *Prox1* clearly plays important roles in the postnatal differentiation of CGE-derived interneurons, the phenotypes we observed in the CR/VIP-expressing bipolar interneuron population when *Prox1* is removed embryonically (*Dlx6a-Cre*) versus postnatally (*Vip-Cre*) are quite distinct.

This raises the possibility that the bipolar subtype is particularly sensitive to its laminar positioning (Figs. 2I, 4I). Alternatively, independent of its role in cell migration, *Prox1* could directly regulate the genetic program required during embryogenesis for bipolar interneurons to properly differentiate and acquire their characteristic morphologies. To distinguish between these possibilities, we dissected out the CGE from control or *Prox1* loss-of-function (*Dlx6a-Cre*; *Prox1-C:EGFP/+* or */F*) embryos at E14.5. We then dissociated and transplanted these cells into wild-type postnatal cortices (P3) and analyzed later at P21 (Fig. 8A). This heterochronic transplantation approach allowed us to bypass the tangential migratory phase of CGE-derived interneuron precursors and to directly test the ability of mutant cells to differentiate within the postnatal cortex. Similar experiments using MGE-derived interneuron precursors have shown that these neurons can properly mature and integrate within the network (Martínez-Cerdeno et al., 2010) when they are heterochronically transplanted into the postnatal cortex (Wonders et al., 2008; Southwell et al., 2010; Inan et al., 2012).

In our control transplantation experiments, we observed EGFP-labeled cells that express VIP-single (without CR; Fig. 8B) or both CR and VIP (Fig. 8C,D) in a proportion similar to those observed in control brains where cells have tangentially migrated from the CGE into the cortex (Fig. 8I, compare the control bars; data without transplantation is shown in proportion from Fig. 4J). In addition, many of these transplanted control cells acquired bipolar morphologies by P21 (Fig. 8B–D). This demonstrates that VIP-expressing CGE-derived interneuron subtype can differentiate properly within the developing cortical plate even without following the normal migratory route from the CGE. However, when E14.5 *Prox1* loss-of-function cells were transplanted, the proportion of EGFP-labeled cells coexpressing CR and VIP was reduced to one-third of that in controls (Fig. 8I, shaded bar graph, right), and their bipolar morphologies were severely attenuated (Fig. 8G,H). These results were comparable to what we observed at P21 in the embryonic *Prox1* loss-of-function mutants (*Dlx6a-Cre*; *Prox1-C:EGFP/F*; Fig. 8I, compare shaded bar graphs of *Prox1* loss-of-function). These results indicate that the severe phenotype in CR/VIP coexpressing bipolar interneurons that we observed in *Prox1* embryonic (*Dlx6a-Cre*) loss-of-function animals was not due to impaired migration and displacement of cells but rather arose directly from an intrinsic requirement for *Prox1* function during interneuron specification. Thus we conclude that *Prox1* independently regulates both the migration and differentiation of CGE-derived cortical interneuron subtypes in a cell-autonomous manner.

Discussion

Despite the recognition that 30% of all GABAergic cortical interneurons originate from the CGE, to date, a specific transcriptional program that selectively regulates the development of these populations has not yet been identified. Moreover, while CGE-derived interneurons display unique patterns of tangential and radial migration and preferentially populate the superficial layers of the cortex, identification of a molecular program that controls

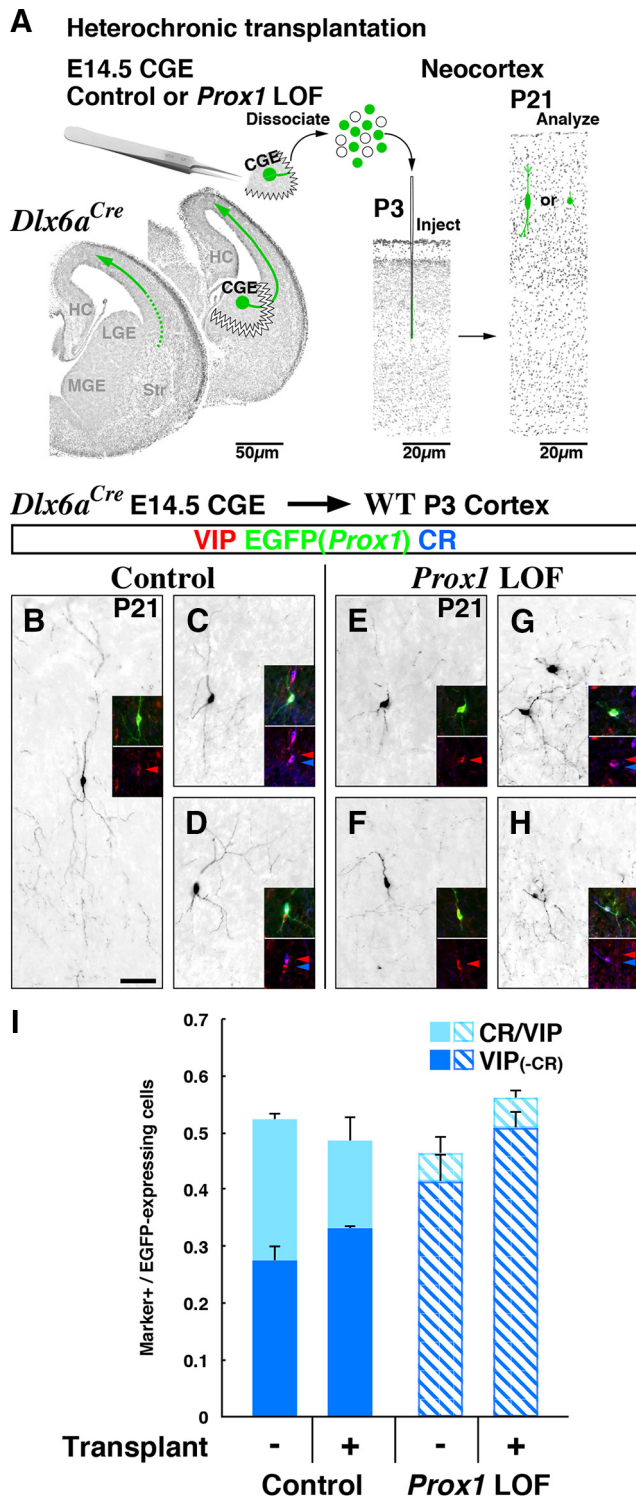


Figure 8. Cell migration and bipolar differentiation of CR/VIP-expressing interneurons is independently and cell-autonomously controlled by *Prox1*. **A**, A schematic of heterochronic transplantation experiments. E14.5 CGE tissue from *Dlx6a-Cre* control and *Prox1* conditional loss-of-function (LOF) embryos (*Prox1-C:EGFP/+* and */F*) was dissected, dissociated, and subsequently transplanted into WT host P3 cortices, allowing CGE-derived interneuron precursors to bypass the tangential migration phase and to directly differentiate inside the cortical plate. **B–D**, Representative examples of transplanted control EGFP(*Prox1*)-labeled cells at P21 that are positive for VIP-single (**B**) or CR/VIP (**C, D**) with EGFP labeling shown in black. **E–H**, *Prox1* loss-of-function EGFP-labeled transplanted cells positive for VIP-single (**E, F**) or CR/VIP (**G, H**) at P21. Transplantation did not rescue the embryonic (*Dlx6a-Cre*) *Prox1* loss-of-function phenotype, as only a few EGFP(*Prox1*)-labeled mutant cells expressed CR/VIP and these did not possess the characteristic bipolar morphologies of this subtype (**G, H**).

these events is lacking. Here, we demonstrate that the homeodomain transcription factor *Prox1*, while initially broadly expressed within the ganglionic eminences, becomes restricted to postmitotic CGE-derived cortical interneuron precursors and is selectively maintained within this population into adulthood. Despite its relatively uniform expression within CGE-derived interneurons, *Prox1* function is differentially required during both embryonic and postnatal stages of development and within distinct subtypes of CGE-derived interneurons (Fig. 9). During cell migration, *Prox1* regulates the integration of CGE-derived interneurons into the superficial cortical layers by coordinating their transition from the subventricular/intermediate zone stream into the cortical plate. The cortical neurogliaform and dense plexus interneuron populations (RELN-positive) are reduced to 40% without *Prox1* function. Furthermore, *Prox1* is cell-autonomously required for the morphological development/maintenance of the CR/VIP-bipolar subtype and proper network integration of VIP-single population. As such, *Prox1* is the first transcription factor to be identified that is specifically required for the differentiation, circuit integration, and maintenance of CGE-derived cortical interneurons.

***Prox1* is selectively maintained in CGE-derived cortical interneuron lineages**

While *Prox1* is initially present in the subventricular zones of all ganglionic eminences, its expression is maintained only in CGE-derived but not MGE-derived cortical interneuron precursors during their respective migration and maturation. What mediates the selective persistence of *Prox1* expression within CGE-derived cortical interneurons? It has been recently demonstrated that canonical β -catenin (*Ctnnb1*)-dependent Wnt signaling controls the expression of *Prox1* in the pallidum. Overexpression of a constitutively active form of β -catenin induces *Prox1* expression uniformly within pyramidal neurons (Machon et al., 2007; Karalay et al., 2011). Conversely, perturbation of canonical Wnt signaling by misexpression of dominant-negative *Lef1* (Karalay et al., 2011) increased Fgf signaling (Shimogori et al., 2004) or *Zeb2* loss-of-function (Miquelajauregui et al., 2007) eliminated *Prox1* expression within the dentate gyrus. Nevertheless, neither gain- nor loss-of-function manipulation of β -catenin activity in the GABAergic population targeted by the *Dlx6a-Cre* driver altered the pattern of *Prox1* expression in MGE- and CGE-derived cortical interneuron precursors at E18.5 (data not shown). As such, to date the only demonstrated role for canonical Wnt signaling in cortical interneuron generation is in the regulation of cell proliferation within the MGE (Gulacsi and Anderson, 2008). These findings indicate that canonical Wnt signaling does not regulate *Prox1* expression within CGE-derived interneurons. In the future, it will be interesting to explore how *Prox1* is differentially regulated within the distinct lineages of cortical interneuron precursors.

In addition to the MGE and CGE, the POA has been shown to give rise to cortical GABAergic interneurons (Bartolini et al., 2013; Miyoshi et al., 2013). The POA harbors at least two distinct progenitor domains that can be delineated by *Nkx5-1* and *Dbx1*

I, Bar graphs representing the proportion of CR/VIP or VIP-single-labeled populations in cells labeled by EGFP(*Prox1*) expression. The values obtained from the heterochronic transplantation experiments (transplant+) resembled the results without transplantation (transplant-; see also Fig. 4J) for both control and *Prox1* loss-of-function. Two-tailed *t* test for transplant-negative versus positive: *p* = 0.191(VIP control), *p* = 0.264(CR/VIP control), *p* = 0.129(VIP mutant), *p* = 0.628(CR/VIP mutant). Error bars represent SEM. Scale bar, 50 µm.

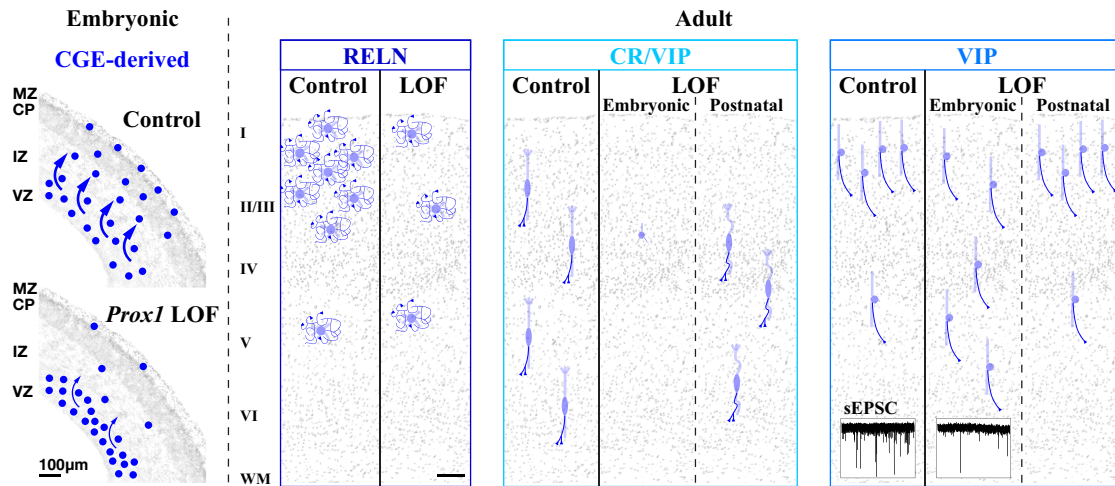


Figure 9. *Prox1* regulates multiple developmental steps of CGE-derived interneurons in a subtype-specific manner. Left, Embryonic, *Prox1* is selectively expressed within CGE-derived cortical interneuron precursors. During embryonic stages, *Prox1* facilitates the transition of tangentially migrating cells from the intermediate zone (IZ) into the cortical plate (CP) and marginal zone (MZ). This step is critical for the positioning of CGE-derived interneuron precursors into the superficial layers of the neocortex. Adult, Embryonic (*Dlx6a-Cre*) and postnatal (*Vip-Cre*) loss-of-function studies reveal that *Prox1* function is differentially required in a stage- and subtype-specific manner. (1) RELN-positive cells were reduced by ~40%. (2) CR/VIP double-positive cells were mostly eliminated from the cortex and the remaining cells failed to acquire their characteristic bipolar morphology. Sustained expression of *Prox1* during postnatal stages is required for the maintenance and survival of this cell class. (3) The VIP-single population was displaced into deep cortical layers. *Prox1* is further required for this interneuron class to receive proper excitatory inputs and to integrate into superficial neocortical circuits. LOF, loss-of-function; VZ, ventricular zone.

expression. POA-derived interneurons originating from an *Nkx5-1* lineage have been fate mapped using a *Nkx5-1BAC-Cre* driver line, and while one-third of this population expresses NPY (Gelman et al., 2009), none of these interneurons were found to express PV, SST, VIP, or CR (Calb2). Interestingly, *Prox1* expression was observed in this POA-derived population (Rubin and Kessaris, 2013). A second POA-derived interneuron population can be fate mapped using the *Dbx1-Cre* driver, and this population gives rise to interneuron classes with the molecular profiles including PV, SST, RELN, and VIP (Gelman et al., 2011). In contrast to the *Nkx5-1*-expressing POA lineage, *Prox1* does not appear to be expressed in the majority of the mature *Dbx1-Cre* fate-mapped population since *Prox1*-positive interneurons express neither PV nor SST (Fig. 1K). To further test if *Prox1* plays any roles in the differentiation and maturation of POA-derived interneurons, it may be interesting to use the *Nkx5-1BAC-Cre* and *Dbx1-Cre* lines to remove *Prox1* in future studies.

Our findings demonstrate a sustained requirement for *Prox1* throughout the development of CGE-derived cortical interneurons. In this regard, *Prox1* is similar to *Dlx1*, which promotes both the embryonic migration of interneuron precursors and the postnatal maintenance of SST-expressing and VIP-expressing interneuron subtypes (Cobos et al., 2005b, 2007). However, our microarray analysis comparing gene expression levels in control versus *Prox1* loss-of-function CGE-derived cells purified from the E18.5 cortex (Table 3) did not reveal any measurable change in *Dlx*-gene family members as well as their known target genes (*Pak3* and *Arx*). We conclude that *Dlx1* and *Prox1* transcription factors independently promote the migration of CGE-derived interneurons through distinct mechanisms.

Distinct requirements for *Prox1* and neuronal activity in the maturation of CGE-derived interneuron subtypes

It has been recently reported that neuronal activity is required for multiple aspects of GABAergic interneuron development (Lin et

al., 2008; Bortone and Polleux, 2009; De Marco García et al., 2011; Inada et al., 2011; Inamura et al., 2012). Within the CGE-derived interneuron populations, suppression of cell activity impairs the migration and morphological development of the RELN-expressing and CR/VIP-expressing subtypes, whereas the VIP-single (CR-negative) class was not affected by this manipulation (De Marco García et al., 2011, 2015; Karayannis et al., 2012).

Here, we find that VIP-single (CR-negative) interneurons require *Prox1* during embryonic stages for proper laminar positioning and for receiving proper levels of excitatory input, even though these cells exhibit relatively normal morphological development in the absence of *Prox1*. Since suppression of activity itself does not affect the formation of excitatory inputs onto VIP-single cells (Karayannis et al., 2012), *Prox1* appears to regulate the circuit integration of this cell type in an activity-independent manner. In contrast, while excitatory inputs onto the RELN-expressing interneuron class were not affected by loss of *Prox1*, intrinsic activity is required for this cell type to receive inputs with the proper kinetics (Karayannis et al., 2012). Our results support the idea that each of the CGE-derived interneuron subtypes is dependent on fundamentally distinct developmental programs that are driven to different extents by a *Prox1*-mediated genetic cascade and intrinsic-activity driven programs (West and Greenberg, 2011). Thus it appears that *Prox1* and neuronal activity independently play essential roles in mediating the connectivity of all CGE-derived interneurons in a subtype-specific manner.

In summary, we demonstrate that *Prox1* function is required for the laminar positioning and development of all CGE-derived cortical interneurons (Fig. 9). Clearly, however, its actions in directing the development of CGE-derived interneurons are both stage and subtype specific. As such, it will be interesting in future studies to identify the molecular partners that work both in concert and in parallel with *Prox1* to confer distinct CGE-derived interneuron properties.

References

- Anderson SA, Eisenstat DD, Shi L, Rubenstein JL (1997) Interneuron migration from basal forebrain to neocortex: dependence on *Dlx* genes. *Science* 278:474–476. [CrossRef Medline](#)
- Anderson SA, Marín O, Horn C, Jennings K, Rubenstein JL (2001) Distinct cortical migrations from the medial and lateral ganglionic eminences. *Development* 128:353–363. [Medline](#)
- Azim E, Jabaudon D, Fame RM, Macklis JD (2009) *SOX6* controls dorsal progenitor identity and interneuron diversity during neocortical development. *Nat Neurosci* 12:1238–1247. [CrossRef Medline](#)
- Balamotis MA, Tamberg N, Woo YJ, Li J, Davy B, Kohwi-Shigematsu T, Kohwi Y (2012) *Satb1* ablation alters temporal expression of immediate early genes and reduces dendritic spine density during postnatal brain development. *Mol Cell Biol* 32:333–347. [CrossRef Medline](#)
- Bartolini G, Ciceri G, Marín O (2013) Integration of GABAergic interneurons into cortical cell assemblies: lessons from embryos and adults. *Neuron* 79:849–864. [CrossRef Medline](#)
- Batista-Brito R, Fishell G (2009) The developmental integration of cortical interneurons into a functional network. *Curr Top Dev Biol* 87:81–118. [CrossRef Medline](#)
- Batista-Brito R, Rossignol E, Hjerling-Leffler J, Denaxa M, Wegner M, Lefebvre V, Pachnis V, Fishell G (2009) The cell-intrinsic requirement of *Sox6* for cortical interneuron development. *Neuron* 63:466–481. [CrossRef Medline](#)
- Battiste J, Helms AW, Kim EJ, Savage TK, Lagace DC, Mandym CD, Eisch AJ, Miyoshi G, Johnson JE (2007) *Ascl1* defines sequentially generated lineage-restricted neuronal and oligodendrocyte precursor cells in the spinal cord. *Development* 134:285–293. [CrossRef Medline](#)
- Bortone D, Polleux F (2009) *KCC2* expression promotes the termination of cortical interneuron migration in a voltage-sensitive calcium-dependent manner. *Neuron* 62:53–71. [CrossRef Medline](#)
- Butt SJ, Fuccillo M, Nery S, Noctor S, Kriegstein A, Corbin JG, Fishell G (2005) The temporal and spatial origins of cortical interneurons predict their physiological subtype. *Neuron* 48:591–604. [CrossRef Medline](#)
- Butt SJ, Sousa VH, Fuccillo MV, Hjerling-Leffler J, Miyoshi G, Kimura S, Fishell G (2008) The requirement of *Nkx2-1* in the temporal specification of cortical interneuron subtypes. *Neuron* 59:722–732. [CrossRef Medline](#)
- Buzsáki G, Kaila K, Raichle M (2007) Inhibition and brain work. *Neuron* 56:771–783. [CrossRef Medline](#)
- Cai Y, Zhang Q, Wang C, Zhang Y, Ma T, Zhou X, Tian M, Rubenstein JL, Yang Z (2013) Nuclear receptor COUP-TFII-expressing neocortical interneurons are derived from the medial and lateral/caudal ganglionic eminence and define specific subsets of mature interneurons. *J Comp Neurol* 521:479–497. [CrossRef Medline](#)
- Choksi SP, Southall TD, Bossing T, Edoff K, de Wit E, Fischer BE, van Steensel B, Micklem G, Brand AH (2006) *Prospero* acts as a binary switch between self-renewal and differentiation in *Drosophila* neural stem cells. *Dev Cell* 11:775–789. [CrossRef Medline](#)
- Chu Z, Galarreta M, Hestrin S (2003) Synaptic interactions of late-spiking neocortical neurons in layer 1. *J Neurosci* 23:96–102. [Medline](#)
- Close J, Xu H, De Marco García N, Batista-Brito R, Rossignol E, Rudy B, Fishell G (2012) *Satb1* is an activity-modulated transcription factor required for the terminal differentiation and connectivity of medial ganglionic eminence-derived cortical interneurons. *J Neurosci* 32:17690–17705. [CrossRef Medline](#)
- Cobos I, Broccoli V, Rubenstein JL (2005a) The vertebrate ortholog of *Aristaless* is regulated by *Dlx* genes in the developing forebrain. *J Comp Neurol* 483:292–303. [CrossRef Medline](#)
- Cobos I, Calcagnotto ME, Vilaythong AJ, Thwin MT, Noebels JL, Baraban SC, Rubenstein JL (2005b) Mice lacking *Dlx1* show subtype-specific loss of interneurons, reduced inhibition and epilepsy. *Nat Neurosci* 8:1059–1068. [CrossRef Medline](#)
- Cobos I, Borello U, Rubenstein JL (2007) *Dlx* transcription factors promote migration through repression of axon and dendrite growth. *Neuron* 54:873–888. [CrossRef Medline](#)
- Colasante G, Collombat P, Raimondi V, Bonanomi D, Ferrai C, Maira M, Yoshikawa K, Mansouri A, Valtorta F, Rubenstein JL, Broccoli V (2008) *Arx* is a direct target of *Dlx2* and thereby contributes to the tangential migration of GABAergic interneurons. *J Neurosci* 28:10674–10686. [CrossRef Medline](#)
- Cook T, Pichaud F, Sonnevill R, Papatsenko D, Desplan C (2003) Distinction between color photoreceptor cell fates is controlled by *Prospero* in *Drosophila*. *Dev Cell* 4:853–864. [CrossRef Medline](#)
- De Marco García NV, Karayannis T, Fishell G (2011) Neuronal activity is required for the development of specific cortical interneuron subtypes. *Nature* 472:351–355. [CrossRef Medline](#)
- De Marco García NV, Priya R, Tuncdemir SN, Fishell G, Karayannis T (2015) Sensory inputs control the integration of neurogliaform interneurons into cortical circuits. *Nat Neurosci* 18:393–401. [CrossRef Medline](#)
- DeFelipe J, López-Cruz PL, Benavides-Piccione R, Bielza C, Larrañaga P, Anderson S, Burkhalter A, Cauli B, Fairén A, Feldmeyer D, Fishell G, Fitzpatrick D, Freund TF, González-Burgos G, Hestrin S, Hill S, Hof PR, Huang J, Jones EG, Kawaguchi Y, et al. (2013) New insights into the classification and nomenclature of cortical GABAergic interneurons. *Nat Rev Neurosci* 14:202–216. [CrossRef Medline](#)
- Denaxa M, Kalaitzidou M, Garefalaki A, Achimastou A, Lasrado R, Maes T, Pachnis V (2012) Maturation-promoting activity of *SATB1* in MGE-derived cortical interneurons. *Cell Rep* 2:1351–1362. [CrossRef Medline](#)
- Doe CQ (2008) Neural stem cells: balancing self-renewal with differentiation. *Development* 135:1575–1587. [CrossRef Medline](#)
- Du T, Xu Q, Ocbina PJ, Anderson SA (2008) *NKX2.1* specifies cortical interneuron fate by activating *Lhx6*. *Development* 135:1559–1567. [CrossRef Medline](#)
- Dyer MA, Livesey FJ, Cepko CL, Oliver G (2003) *Prox1* function controls progenitor cell proliferation and horizontal cell genesis in the mammalian retina. *Nat Genet* 34:53–58. [CrossRef Medline](#)
- Dymecki SM, Kim JC (2007) Molecular neuroanatomy's "Three Gs": a primer. *Neuron* 54:17–34. [CrossRef Medline](#)
- Fairén A, Cobas A, Fonseca M (1986) Times of generation of glutamic acid decarboxylase immunoreactive neurons in mouse somatosensory cortex. *J Comp Neurol* 251:67–83. [CrossRef Medline](#)
- Fino E, Packer AM, Yuste R (2013) The logic of inhibitory connectivity in the neocortex. *Neuroscientist* 19:228–237. [CrossRef Medline](#)
- Flames N, Pla R, Gelman DM, Rubenstein JL, Puelles L, Marín O (2007) Delineation of multiple subpallial progenitor domains by the combinatorial expression of transcriptional codes. *J Neurosci* 27:9682–9695. [CrossRef Medline](#)
- Flandin P, Kimura S, Rubenstein JL (2010) The progenitor zone of the ventral medial ganglionic eminence requires *Nkx2-1* to generate most of the globus pallidus but few neocortical interneurons. *J Neurosci* 30:2812–2823. [CrossRef Medline](#)
- Fogarty M, Grist M, Gelman D, Marín O, Pachnis V, Kessaris N (2007) Spatial genetic patterning of the embryonic neuroepithelium generates GABAergic interneuron diversity in the adult cortex. *J Neurosci* 27:10935–10946. [CrossRef Medline](#)
- Franco SJ, Müller U (2013) Shaping our minds: stem and progenitor cell diversity in the mammalian neocortex. *Neuron* 77:19–34. [CrossRef Medline](#)
- Franco SJ, Martínez-Garay I, Gil-Sanz C, Harkins-Perry SR, Müller U (2011) *Reelin* regulates cadherin function via *Dab1/Rap1* to control neuronal migration and lamination in the neocortex. *Neuron* 69:482–497. [CrossRef Medline](#)
- Friocourt G, Kanatani S, Tabata H, Yozu M, Takahashi T, Antypa M, Raguénès O, Chelly J, Férec C, Nakajima K, Parnavelas JG (2008) Cell-autonomous roles of *ARX* in cell proliferation and neuronal migration during corticogenesis. *J Neurosci* 28:5794–5805. [CrossRef Medline](#)
- Gao P, Sultan KT, Zhang XJ, Shi SH (2013) Lineage-dependent circuit assembly in the neocortex. *Development* 140:2645–2655. [CrossRef Medline](#)
- Gelman DM, Marín O (2010) Generation of interneuron diversity in the mouse cerebral cortex. *Eur J Neurosci* 31:2136–2141. [CrossRef Medline](#)
- Gelman DM, Martini FJ, Nóbrega-Pereira S, Pierani A, Kessaris N, Marín O (2009) The embryonic preoptic area is a novel source of cortical GABAergic interneurons. *J Neurosci* 29:9380–9389. [CrossRef Medline](#)
- Gelman D, Griveau A, Dehorter N, Teissier A, Varela C, Pla R, Pierani A, Marín O (2011) A wide diversity of cortical GABAergic interneurons derives from the embryonic preoptic area. *J Neurosci* 31:16570–16580. [CrossRef Medline](#)
- Gil-Sanz C, Franco SJ, Martínez-Garay I, Espinosa A, Harkins-Perry S, Müller U (2013) Cajal-Retzius cells instruct neuronal migration by coincidence signaling between secreted and contact-dependent guidance cues. *Neuron* 79:461–477. [CrossRef Medline](#)
- Gong S, Zheng C, Doughty ML, Losos K, Didkovsky N, Schambra UB, Nowak NJ, Joyner A, Leblanc G, Hatten ME, Heintz N (2003) A gene expression atlas of the central nervous system based on bacterial artificial chromosomes. *Nature* 425:917–925. [CrossRef Medline](#)
- Gulacsi AA, Anderson SA (2008) *Beta-catenin*-mediated *Wnt* signaling regulates neurogenesis in the ventral telencephalon. *Nat Neurosci* 11:1383–1391. [CrossRef Medline](#)
- Harvey NL, Srinivasan RS, Dillard ME, Johnson NC, Witte MH, Boyd K,

- Sleeman MW, Oliver G (2005) Lymphatic vascular defects promoted by *Prox1* haploinsufficiency cause adult-onset obesity. *Nat Genet* 37:1072–1081. [CrossRef Medline](#)
- Hernández-Miranda LR, Parnavelas JG, Chiara F (2010) Molecules and mechanisms involved in the generation and migration of cortical interneurons. *ASN Neuro* 2:e00031. [CrossRef Medline](#)
- Inada H, Watanabe M, Uchida T, Ishibashi H, Wake H, Nemoto T, Yanagawa Y, Fukuda A, Nabekura J (2011) GABA regulates the multidirectional tangential migration of GABAergic interneurons in living neonatal mice. *PLoS One* 6:e27048. [CrossRef Medline](#)
- Inamura N, Kimura T, Tada S, Kurahashi T, Yanagida M, Yanagawa Y, Ike-naka K, Murakami F (2012) Intrinsic and extrinsic mechanisms control the termination of cortical interneuron migration. *J Neurosci* 32:6032–6042. [CrossRef Medline](#)
- Inan M, Welagen J, Anderson SA (2012) Spatial and temporal bias in the mitotic origins of somatostatin- and parvalbumin-expressing interneuron subgroups and the chandelier subtype in the medial ganglionic eminence. *Cereb Cortex* 22:820–827. [CrossRef Medline](#)
- Isaacson JS, Scanziani M (2011) How inhibition shapes cortical activity. *Neuron* 72:231–243. [CrossRef Medline](#)
- Iwano T, Masuda A, Kiyonari H, Enomoto H, Matsuzaki F (2012) *Prox1* postmitotically defines dentate gyrus cells by specifying granule cell identity over CA3 pyramidal cell fate in the hippocampus. *Development* 139:3051–3062. [CrossRef Medline](#)
- Kaltezioti V, Kouroupi G, Oikonomaki M, Mantouvalou E, Stergiopoulos A, Charonis A, Rohrer H, Matsas R, Politis PK (2010) *Prox1* regulates the notch1-mediated inhibition of neurogenesis. *PLoS Biol* 8:e1000565. [CrossRef Medline](#)
- Kanatani S, Yozu M, Tabata H, Nakajima K (2008) COUP-TFII is preferentially expressed in the caudal ganglionic eminence and is involved in the caudal migratory stream. *J Neurosci* 28:13582–13591. [CrossRef Medline](#)
- Karalay O, Doberauer K, Vadodaria KC, Knobloch M, Berti L, Miquelajaugui A, Schwark M, Jagasia R, Taketo MM, Tarabykin V, Lie DC, Jessberger S (2011) Prospero-related homeobox 1 gene (*Prox1*) is regulated by canonical Wnt signaling and has a stage-specific role in adult hippocampal neurogenesis. *Proc Natl Acad Sci U S A* 108:5807–5812. [CrossRef Medline](#)
- Karayannis T, De Marco García NV, Fishell GJ (2012) Functional adaptation of cortical interneurons to attenuated activity is subtype-specific. *Front Neural Circuits* 6:66. [CrossRef Medline](#)
- Kessaris N, Fogarty M, Iannarelli P, Grist M, Wegner M, Richardson WD (2006) Competing waves of oligodendrocytes in the forebrain and postnatal elimination of an embryonic lineage. *Nat Neurosci* 9:173–179. [CrossRef Medline](#)
- Kessaris N, Magno L, Rubin AN, Oliveira MG (2014) Genetic programs controlling cortical interneuron fate. *Curr Opin Neurobiol* 26:79–87. [CrossRef Medline](#)
- Klausberger T, Somogyi P (2008) Neuronal diversity and temporal dynamics: the unity of hippocampal circuit operations. *Science* 321:53–57. [CrossRef Medline](#)
- Kriegstein AR, Noctor SC (2004) Patterns of neuronal migration in the embryonic cortex. *Trends Neurosci* 27:392–399. [CrossRef Medline](#)
- Krook-Magnuson E, Varga C, Lee SH, Soltesz I (2012) New dimensions of interneuronal specialization unmasked by principal cell heterogeneity. *Trends Neurosci* 35:175–184. [CrossRef Medline](#)
- Kubota Y, Hattori R, Yui Y (1994) Three distinct subpopulations of GABAergic neurons in rat frontal agranular cortex. *Brain Res* 649:159–173. [CrossRef Medline](#)
- Kubota Y, Shigematsu N, Karube F, Sekigawa A, Kato S, Yamaguchi N, Hirai Y, Morishima M, Kawaguchi Y (2011) Selective coexpression of multiple chemical markers defines discrete populations of neocortical GABAergic neurons. *Cereb Cortex* 21:1803–1817. [CrossRef Medline](#)
- Kvitsiani D, Ranade S, Hangya B, Taniguchi H, Huang JZ, Kepecs A (2013) Distinct behavioural and network correlates of two interneuron types in prefrontal cortex. *Nature* 498:363–366. [CrossRef Medline](#)
- Kwan KY, Sestan N, Anton ES (2012) Transcriptional co-regulation of neuronal migration and laminar identity in the neocortex. *Development* 139:1535–1546. [CrossRef Medline](#)
- Larkum M (2013) A cellular mechanism for cortical associations: an organizing principle for the cerebral cortex. *Trends Neurosci* 36:141–151. [CrossRef Medline](#)
- Lavado A, Oliver G (2007) *Prox1* expression patterns in the developing and adult murine brain. *Dev Dyn* 236:518–524. [CrossRef Medline](#)
- Lavado A, Lagutin OV, Chow LM, Baker SJ, Oliver G (2010) *Prox1* is required for granule cell maturation and intermediate progenitor maintenance during brain neurogenesis. *PLoS Biol* 8:e1000460. [CrossRef Medline](#)
- Lee S, Hjerling-Leffler J, Zagha E, Fishell G, Rudy B (2010) The largest group of superficial neocortical GABAergic interneurons expresses ionotropic serotonin receptors. *J Neurosci* 30:16796–16808. [CrossRef Medline](#)
- Le Magueresse C, Monyer H (2013) GABAergic interneurons shape the functional maturation of the cortex. *Neuron* 77:388–405. [CrossRef Medline](#)
- Leone DP, Srinivasan K, Chen B, Alcamo E, McConnell SK (2008) The determination of projection neuron identity in the developing cerebral cortex. *Curr Opin Neurobiol* 18:28–35. [CrossRef Medline](#)
- Li G, Adesnik H, Li J, Long J, Nicoll RA, Rubenstein JL, Pleasure SJ (2008) Regional distribution of cortical interneurons and development of inhibitory tone are regulated by *Cxcl12/Cxcr4* signaling. *J Neurosci* 28:1085–1098. [CrossRef Medline](#)
- Lin Y, Bloodgood BL, Hauser JL, Lapan AD, Koon AC, Kim TK, Hu LS, Malik AN, Greenberg ME (2008) Activity-dependent regulation of inhibitory synapse development by *Npas4*. *Nature* 455:1198–1204. [CrossRef Medline](#)
- Liodis P, Denaxa M, Grigoriou M, Akufo-Addo C, Yanagawa Y, Pachnis V (2007) *Lhx6* activity is required for the normal migration and specification of cortical interneuron subtypes. *J Neurosci* 27:3078–3089. [CrossRef Medline](#)
- Lodato S, Tomassy GS, De Leonibus E, Uzcategui YG, Andolfi G, Armentano M, Touzot A, Gaztelu JM, Arlotta P, Menendez de la Prida L, Studer M (2011) Loss of COUP-TFI alters the balance between caudal ganglionic eminence- and medial ganglionic eminence-derived cortical interneurons and results in resistance to epilepsy. *J Neurosci* 31:4650–4662. [CrossRef Medline](#)
- López-Bendito G, Sánchez-Alcaniz JA, Pla R, Borrell V, Picó E, Valdeolmillos M, Marín O (2008) Chemokine signaling controls intracortical migration and final distribution of GABAergic interneurons. *J Neurosci* 28:1613–1624. [CrossRef Medline](#)
- Lui JH, Hansen DV, Kriegstein AR (2011) Development and evolution of the human neocortex. *Cell* 146:18–36. [CrossRef Medline](#)
- Ma J, Yao XH, Fu Y, Yu YC (2014) Development of layer I neurons in the mouse neocortex. *Cereb Cortex* 24:2604–2618. [CrossRef Medline](#)
- Ma T, Zhang Q, Cai Y, You Y, Rubenstein JL, Yang Z (2012) A subpopulation of dorsal lateral/caudal ganglionic eminence-derived neocortical interneurons expresses the transcription factor *Sp8*. *Cereb Cortex* 22:2120–2130. [CrossRef Medline](#)
- Machon O, Backman M, Machonova O, Kozmik Z, Vacik T, Andersen L, Krauss S (2007) A dynamic gradient of Wnt signaling controls initiation of neurogenesis in the mammalian cortex and cellular specification in the hippocampus. *Dev Biol* 311:223–237. [CrossRef Medline](#)
- Madisen L, Zwingman TA, Sunkin SM, Oh SW, Zariwala HA, Gu H, Ng LL, Palminter RD, Hawrylycz MJ, Jones AR, Lein ES, Zeng H (2010) A robust and high-throughput Cre reporting and characterization system for the whole mouse brain. *Nat Neurosci* 13:133–140. [CrossRef Medline](#)
- Marín O (2013) Cellular and molecular mechanisms controlling the migration of neocortical interneurons. *Eur J Neurosci* 38:2019–2029. [CrossRef Medline](#)
- Marín O, Rubenstein JL (2003) Cell migration in the forebrain. *Annu Rev Neurosci* 26:441–483. [CrossRef Medline](#)
- Marín O, Valiente M, Ge X, Tsai LH (2010) Guiding neuronal cell migrations. *Cold Spring Harb Perspect Biol* 2:a001834. [CrossRef Medline](#)
- Markram H, Toledo-Rodriguez M, Wang Y, Gupta A, Silberberg G, Wu C (2004) Interneurons of the neocortical inhibitory system. *Nat Rev Neurosci* 5:793–807. [CrossRef Medline](#)
- Martínez-Cerdeno V, Noctor SC, Espinosa A, Ariza J, Parker P, Orasji S, Daadi MM, Bankiewicz K, Alvarez-Buylla A, Kriegstein AR (2010) Embryonic MGE precursor cells grafted into adult rat striatum integrate and ameliorate motor symptoms in 6-OHDA-lesioned rats. *Cell Stem Cell* 6:238–250. [CrossRef Medline](#)
- Métin C, Alvarez C, Moudoux D, Vitalis T, Pieau C, Molnár Z (2007) Conserved pattern of tangential neuronal migration during forebrain development. *Development* 134:2815–2827. [CrossRef Medline](#)
- Miller MW (1985) Cogeneration of retrogradely labeled corticocortical projection and GABA-immunoreactive local circuit neurons in cerebral cortex. *Brain Res* 355:187–192. [CrossRef Medline](#)
- Miquelajaugui A, Van de Putte T, Polyakov A, Nityanandam A, Boppana S, Seuntjens E, Karabinos A, Higashi Y, Huylebroeck D, Tarabykin V

- (2007) Smad-interacting protein-1 (*Zfh1b*) acts upstream of Wnt signaling in the mouse hippocampus and controls its formation. *Proc Natl Acad Sci U S A* 104:12919–12924. [CrossRef Medline](#)
- Miyoshi G, Fishell G (2006) Directing neuron-specific transgene expression in the mouse CNS. *Curr Opin Neurobiol* 16:577–584. [CrossRef Medline](#)
- Miyoshi G, Fishell G (2011) GABAergic interneuron lineages selectively sort into specific cortical layers during early postnatal development. *Cereb Cortex* 21:845–852. [CrossRef Medline](#)
- Miyoshi G, Fishell G (2012) Dynamic FoxG1 expression coordinates the integration of multipolar pyramidal neuron precursors into the cortical plate. *Neuron* 74:1045–1058. [CrossRef Medline](#)
- Miyoshi G, Butt SJ, Takebayashi H, Fishell G (2007) Physiologically distinct temporal cohorts of cortical interneurons arise from telencephalic Olig2-expressing precursors. *J Neurosci* 27:7786–7798. [CrossRef Medline](#)
- Miyoshi G, Hjerling-Leffler J, Karayannis T, Sousa VH, Butt SJ, Battiste J, Johnson JE, Machold RP, Fishell G (2010) Genetic fate mapping reveals that the caudal ganglionic eminence produces a large and diverse population of superficial cortical interneurons. *J Neurosci* 30:1582–1594. [CrossRef Medline](#)
- Miyoshi G, Machold RP, Fishell G (2013) Specification of GABAergic neocortical interneurons. In: *Cortical development: neural diversity and neocortical organization*, pp 89–126. Tokyo: Springer Japan.
- Molynieux BJ, Arlotta P, Menezes JR, Macklis JD (2007) Neuronal subtype specification in the cerebral cortex. *Nat Rev Neurosci* 8:427–437. [CrossRef Medline](#)
- Monory K, Massa F, Egertová M, Eder M, Blaudzun H, Westenbroek R, Kelsch W, Jacob W, Marsch R, Ekker M, Long J, Rubenstein JL, Goebbels S, Nave KA, Düring M, Klugmann M, Wölfel B, Dodt HU, Zieglgänsberger W, Wotjak CT, et al. (2006) The endocannabinoid system controls key epileptogenic circuits in the hippocampus. *Neuron* 51:455–466. [CrossRef Medline](#)
- Murthy S, Niquire M, Hurni N, Limoni G, Frazer S, Chameau P, van Hooft JA, Vitalis T, Dayer A (2014) Serotonin receptor 3A controls interneuron migration into the neocortex. *Nat Commun* 5:5524. [CrossRef Medline](#)
- Nadarajah B, Alifragis P, Wong RO, Parnavelas JG (2002) Ventricle-directed migration in the developing cerebral cortex. *Nat Neurosci* 5:218–224. [CrossRef Medline](#)
- Narboux-Nême N, Goïame R, Mattéi MG, Cohen-Tannoudji M, Wassef M (2012) Integration of H-2Z1, a somatosensory cortex-expressed transgene, interferes with the expression of the *Satb1* and *Tbc1d5* flanking genes and affects the differentiation of a subset of cortical interneurons. *J Neurosci* 32:7287–7300. [CrossRef Medline](#)
- Nery S, Fishell G, Corbin JG (2002) The caudal ganglionic eminence is a source of distinct cortical and subcortical cell populations. *Nat Neurosci* 5:1279–1287. [CrossRef Medline](#)
- Nóbrega-Pereira S, Gelman D, Bartolini G, Pla R, Pierani A, Marín O (2010) Origin and molecular specification of globus pallidus neurons. *J Neurosci* 30:2824–2834. [CrossRef Medline](#)
- Pohlkamp T, Dávid C, Cauli B, Gallopin T, Bouché E, Karagiannis A, May P, Herz J, Frotscher M, Staiger JF, Bock HH (2014) Characterization and distribution of reelin-positive interneuron subtypes in the rat barrel cortex. *Cereb Cortex* 24:3046–3058. [CrossRef Medline](#)
- Rakic P (2009) Evolution of the neocortex: a perspective from developmental biology. *Nat Rev Neurosci* 10:724–735. [CrossRef Medline](#)
- Rubin AN, Kessaris N (2013) PROX1: a lineage tracer for cortical interneurons originating in the lateral/caudal ganglionic eminence and preoptic area. *PLoS One* 8:e77339. [CrossRef Medline](#)
- Rubin AN, Alfonsi F, Humphreys MP, Choi CK, Rocha SF, Kessaris N (2010) The germinal zones of the basal ganglia but not the septum generate GABAergic interneurons for the cortex. *J Neurosci* 30:12050–12062. [CrossRef Medline](#)
- Rymar VV, Sadikot AF (2007) Laminal fate of cortical GABAergic interneurons is dependent on both birthdate and phenotype. *J Comp Neurol* 501:369–380. [CrossRef Medline](#)
- Sessa A, Mao CA, Colasante G, Nini A, Klein WH, Broccoli V (2010) Tbr2-positive intermediate (basal) neuronal progenitors safeguard cerebral cortex expansion by controlling amplification of pallial glutamatergic neurons and attraction of subpallial GABAergic interneurons. *Genes Dev* 24:1816–1826. [CrossRef Medline](#)
- Shimogori T, Banuchi V, Ng HY, Strauss JB, Grove EA (2004) Embryonic signaling centers expressing BMP, WNT and FGF proteins interact to pattern the cerebral cortex. *Development* 131:5639–5647. [CrossRef Medline](#)
- Sohal VS, Zhang F, Yizhar O, Deisseroth K (2009) Parvalbumin neurons and gamma rhythms enhance cortical circuit performance. *Nature* 459:698–702. [CrossRef Medline](#)
- Sousa VH, Miyoshi G, Hjerling-Leffler J, Karayannis T, Fishell G (2009) Characterization of Nkx6-2-derived neocortical interneuron lineages. *Cereb Cortex* 19 [Suppl 1]:i1–i10. [CrossRef Medline](#)
- Southwell DG, Froemke RC, Alvarez-Buylla A, Stryker MP, Gandhi SP (2010) Cortical plasticity induced by inhibitory neuron transplantation. *Science* 327:1145–1148. [CrossRef Medline](#)
- Sussel L, Marin O, Kimura S, Rubenstein JL (1999) Loss of Nkx2.1 homeobox gene function results in a ventral to dorsal molecular respecification within the basal telencephalon: evidence for a transformation of the pallidum into the striatum. *Development* 126:3359–3370. [Medline](#)
- Tamás G, Lorincz A, Simon A, Szabadics J (2003) Identified sources and targets of slow inhibition in the neocortex. *Science* 299:1902–1905. [CrossRef Medline](#)
- Tanaka DH, Nakajima K (2012) Migratory pathways of GABAergic interneurons when they enter the neocortex. *Eur J Neurosci* 35:1655–1660. [CrossRef Medline](#)
- Tanaka DH, Maekawa K, Yanagawa Y, Obata K, Murakami F (2006) Multidirectional and multizonal tangential migration of GABAergic interneurons in the developing cerebral cortex. *Development* 133:2167–2176. [CrossRef Medline](#)
- Taniguchi H, He M, Wu P, Kim S, Paik R, Sugino K, Kvitsiani D, Fu Y, Lu J, Lin Y, Miyoshi G, Shima Y, Fishell G, Nelson SB, Huang ZJ (2011) A resource of Cre driver lines for genetic targeting of GABAergic neurons in cerebral cortex. *Neuron* 71:995–1013. [CrossRef Medline](#)
- Thomson AM, Lamy C (2007) Functional maps of neocortical local circuitry. *Front Neurosci* 1:19–42. [CrossRef Medline](#)
- Torii M, Matsuzaki F, Osumi N, Kaibuchi K, Nakamura S, Casarosa S, Guillemot F, Nakafuku M (1999) Transcription factors Mash-1 and Prox-1 delineate early steps in differentiation of neural stem cells in the developing central nervous system. *Development* 126:443–456. [Medline](#)
- Tripodi M, Filosa A, Armentano M, Studer M (2004) The COUP-TF nuclear receptors regulate cell migration in the mammalian basal forebrain. *Development* 131:6119–6129. [CrossRef Medline](#)
- Vucurovic K, Gallopin T, Ferezou I, Rancillac A, Chameau P, van Hooft JA, Geoffroy H, Monyer H, Rossier J, Vitalis T (2010) Serotonin 3A receptor subtype as an early and protracted marker of cortical interneuron subpopulations. *Cereb Cortex* 20:2333–2347. [CrossRef Medline](#)
- Waclaw RR, Allen ZJ 2nd, Bell SM, Erdélyi F, Szabó G, Potter SS, Campbell K (2006) The zinc finger transcription factor Sp8 regulates the generation and diversity of olfactory bulb interneurons. *Neuron* 49:503–516. [CrossRef Medline](#)
- West AE, Greenberg ME (2011) Neuronal activity-regulated gene transcription in synapse development and cognitive function. *Cold Spring Harb Perspect Biol* 3:a005744. [CrossRef Medline](#)
- Wichterle H, Turnbull DH, Nery S, Fishell G, Alvarez-Buylla A (2001) In utero fate mapping reveals distinct migratory pathways and fates of neurons born in the mammalian basal forebrain. *Development* 128:3759–3771. [Medline](#)
- Wonders CP, Anderson SA (2006) The origin and specification of cortical interneurons. *Nat Rev Neurosci* 7:687–696. [CrossRef Medline](#)
- Wonders CP, Taylor L, Welagen J, Mbata IC, Xiang JZ, Anderson SA (2008) A spatial bias for the origins of interneuron subgroups within the medial ganglionic eminence. *Dev Biol* 314:127–136. [CrossRef Medline](#)
- Xu Q, Cobos I, De La Cruz E, Rubenstein JL, Anderson SA (2004) Origins of cortical interneuron subtypes. *J Neurosci* 24:2612–2622. [CrossRef Medline](#)
- Xu Q, Tam M, Anderson SA (2008) Fate mapping Nkx2.1-lineage cells in the mouse telencephalon. *J Comp Neurol* 506:16–29. [CrossRef Medline](#)
- Yoshida M, Assimacopoulos S, Jones KR, Grove EA (2006) Massive loss of Cajal-Retzius cells does not disrupt neocortical layer order. *Development* 133:537–545. [CrossRef Medline](#)
- Zhao Y, Flandin P, Long JE, Cuesta MD, Westphal H, Rubenstein JL (2008) Distinct molecular pathways for development of telencephalic interneuron subtypes revealed through analysis of Lhx6 mutants. *J Comp Neurol* 510:79–99. [CrossRef Medline](#)